



# Sclerochronological evidence of pronounced seasonality from the late Pliocene of the southern North Sea basin and its implications

Andrew L. A. Johnson<sup>1</sup>, Annemarie M. Valentine<sup>2</sup>, Bernd R. Schöne<sup>3</sup>, Melanie J. Leng<sup>4</sup>, and Stijn Goolaerts<sup>5</sup>

<sup>1</sup>School of Built and Natural Environment, University of Derby, Derby, DE22 1GB, UK

<sup>2</sup>School of Geography and Environmental Science, Nottingham Trent University, Southwell, NG25 0QF, UK

<sup>3</sup>Institute of Geosciences, University of Mainz, 55128 Mainz, Germany

<sup>4</sup>National Environmental Isotope Facility, British Geological Survey, Keyworth, NG12 5GG, UK

<sup>5</sup>OD Earth & History of Life and Scientific Heritage Service, Royal Belgian Institute of Natural Sciences, 1000 Brussels, Belgium

**Correspondence:** Andrew L. A. Johnson (a.l.a.johnson@derby.ac.uk)

Received: 21 October 2021 – Discussion started: 19 November 2021

Revised: 19 April 2022 – Accepted: 22 April 2022 – Published: 30 May 2022

**Abstract.** Oxygen isotope ( $\delta^{18}\text{O}$ ) sclerochronology of benthic marine molluscs provides a means of reconstructing the seasonal range in seafloor temperature, subject to use of an appropriate equation relating shell  $\delta^{18}\text{O}$  to temperature and water  $\delta^{18}\text{O}$ , a reasonably accurate estimation of water  $\delta^{18}\text{O}$ , and due consideration of growth-rate effects. Taking these factors into account,  $\delta^{18}\text{O}$  data from late Pliocene bivalves of the southern North Sea basin (Belgium and the Netherlands) indicate a seasonal seafloor range a little smaller than now in the area. Microgrowth-increment data from *Aequipecten opercularis*, together with the species composition of the bivalve assemblage and aspects of preservation, suggest a setting below the summer thermocline for all but the latest material investigated. This implies a higher summer temperature at the surface than on the seafloor and consequently a greater seasonal range. A reasonable (3 °C) estimate of the difference between maximum seafloor and surface temperature under circumstances of summer stratification points to seasonal surface ranges in excess of the present value (12.4 °C nearby). Using a model-derived estimate of water  $\delta^{18}\text{O}$  (0.0 ‰), summer surface temperature was initially in the cool temperate range (< 20 °C) and then (during the Mid-Piacenzian Warm Period; MPWP) increased into the warm temperate range (> 20 °C) before reverting to cool temperate values (in conjunction with shallowing and a loss of summer stratification). This pattern is in agreement with biotic-

assemblage evidence. Winter temperature was firmly in the cool temperate range (< 10 °C) throughout, contrary to previous interpretations. Averaging of summer and winter surface temperatures for the MPWP provides a figure for annual sea surface temperature that is 2–3 °C higher than the present value (10.9 °C nearby) and in close agreement with a figure obtained by averaging alkenone and TEX<sub>86</sub> temperatures for the MPWP from the Netherlands. These proxies, however, respectively, underestimate summer temperature and overestimate winter temperature, giving an incomplete picture of seasonality. A higher annual temperature than now is consistent with the notion of global warmth in the MPWP, but a low winter temperature in the southern North Sea basin suggests regional reduction in oceanic heat supply, contrasting with other interpretations of North Atlantic oceanography during the interval. Carbonate clumped isotope ( $\Delta_{47}$ ) and biomineral unit thermometry offer means of checking the  $\delta^{18}\text{O}$ -based temperatures.

## 1 Introduction

The foraminiferal  $\delta^{18}\text{O}$  record from the deep sea indicates that the global volume of land ice was generally lower than now during the Pliocene epoch (Lisiecki and Raymo, 2005), and that global mean surface temperature (GMST) was therefore generally higher. The late Pliocene saw the last mainly

warm interval before the change to the typically cooler-than-present conditions of the Pleistocene. During this interval, the Mid-Piacenzian Warm Period (MPWP; 3.28–3.03 Ma; Dowsett et al., 2019), “warm peak average” temperature was 2–3 °C higher than now, similar to the GMST predicted for the end of the present century (Dowsett et al., 2013). As evident under current global warming, the mid-Piacenzian temperature anomaly was not uniform, being for instance greater than the global average figure at midlatitudes in the oceans according to results from both proxies and modelling (Lunt et al., 2010). Despite general agreement, strong discrepancies between proxy and model estimates of mean annual sea surface temperature (ASST) have been identified in some regions (Dowsett et al., 2011). Those formerly recognized in the northern North Atlantic Ocean have been reduced by limiting proxy estimates to one source – alkenone index – and adjusting model boundary conditions (Dowsett et al., 2019). It is, however, widely considered (e.g. Robinson, 2009; Bova et al., 2021) that alkenone index reflects temperature in the warmer part of the year, and the same has now been suggested to be the case for another commonly utilized geochemical proxy, the Mg/Ca ratio of foraminiferal calcite (Bova et al., 2021). The species composition of assemblages of pelagic micro-organisms (particularly Foraminifera) has been extensively used to derive both summer and winter sea surface temperatures for the Pliocene (e.g. Dowsett et al., 2010). The methodology, employing information on the seasonal temperatures associated with modern representatives and relatives, assumes constancy of niche (“ecological uniformitarianism”; Vignols et al., 2019) and, furthermore, that both summer and winter temperatures exert an influence on modern occurrence. This is questionable for the many forms that “bloom” in summer and those (dinoflagellates) that survive winter as cysts (dinocysts).

It would be possible to obtain a more accurate estimate of regional mean ASST for comparison with model outputs by combining temperatures from a summer proxy with those from a winter proxy if such existed. Dearing Crampton-Flood et al. (2020) obtained TEX<sub>86</sub> estimates about 6 °C lower than from alkenones for sea temperature during the MPWP in the Netherlands. They argued from several lines of evidence that the former data reflect surface conditions during winter, when the source organisms (archaea) of the lipids concerned may have bloomed. Given that alkenones (produced by haptophyte algae) seem to reflect summer surface conditions, we could take the midpoint between the TEX<sub>86</sub> and alkenone temperatures as an estimate of mean ASST. However, in the absence of information on the precise times during winter and summer that are represented we could not be sure of the accuracy of the mean ASST estimate, and we would also be unable to say whether the winter and summer figures give a full picture of seasonality. In this paper we use sclerochronology (investigation of the chemical and physical nature of accretionary mineralized skeletons) to obtain estimates of extreme summer and winter sea tempera-

tures in individual years over a late Pliocene interval spanning the MPWP in Belgium and the Netherlands. The information substantially supplements initial sclerochronological estimates (Valentine et al., 2011) from these countries on the eastern side of the southern North Sea basin (SNSB), and complements a sizeable body of equivalent data relating to the early Pliocene (Zanclean) sequence of eastern England, on the western side of the SNSB (Johnson et al., 2009, 2021b; Vignols et al., 2019). The results serve to (1) test estimates of seasonality and annual (average) temperature obtained from other proxies; (2) expand and refine the proxy evidence of temperature available for testing models of Pliocene climate; (3) provide an insight into the controls on regional marine climate.

## 2 Sclerochronology and seasonality

The majority of sclerochronological studies of the environment have been conducted on accretionary calcium carbonate skeletons, principally those of corals and molluscs in the marine realm. Trace element (Sr/Ca) profiles from shallow-water corals have been found to mirror seasonal changes in surface temperature (e.g. DeLong et al., 2007, 2011), but no such close relationship exists in molluscs (e.g. Gillikin et al., 2005; Markulin et al., 2019). In view of the absence of corals (at least long-lived, colonial forms) from extra-tropical shallow-water environments and the general inutility of trace (and minor) element data from molluscs for reconstructing seasonal temperature variation, sclerochronological investigations of palaeoseasonality in temperate and polar settings have been largely based on the  $\delta^{18}\text{O}$  of molluscan carbonate. Pelagic belemnites supplement benthic molluscs as a provider of information on Jurassic and Cretaceous conditions (e.g. Mettam et al., 2014), but after the extinction of the former at the end of the Cretaceous the latter become the sole source of data (e.g. Bice et al., 1996; Williams et al., 2010; Surge and Barrett, 2012; Johnson et al., 2009, 2017, 2019; Vignols et al., 2019; de Winter et al., 2020a, b). There is no doubt that temperature exerts an influence on the  $\delta^{18}\text{O}$  of molluscan carbonate, but values are also affected by the  $\delta^{18}\text{O}$  of the fluid from which the material was precipitated (usually taken to be equivalent to that of ambient water) and by kinetic and more obscure “vital” effects (e.g. Owen et al., 2002a, b; Fenger et al., 2007; Garcia-March et al., 2011). At present it is possible only to constrain (not specify) the  $\delta^{18}\text{O}$  of ambient water in ancient settings, so, although precise, the temperatures from  $\delta^{18}\text{O}$  thermometry are not necessarily accurate – i.e. they are questionable as absolute temperatures. Nevertheless, assuming that kinetic and vital effects do not vary with season or age, an assumption which is certainly valid for some molluscs (e.g. Fenger et al., 2007; Garcia-March et al., 2011), and that water  $\delta^{18}\text{O}$  is constant, ontogenetic profiles are, at least in principle, a true reflection of relative

temperature and hence (from the difference between summer and winter  $\delta^{18}\text{O}$  values) of seasonality.

Unfortunately, molluscan growth is often discontinuous, and interruptions are frequently associated with seasonal temperature extremes (Schöne, 2008), so in such cases the shell  $\delta^{18}\text{O}$  record does not fully reflect the range of temperatures experienced (e.g. Hickson et al., 2000; Peharda et al., 2019a). However, because of their typical manifestation as “growth lines”, interruptions can be recognized and instances of likely truncation of the  $\delta^{18}\text{O}$  record inferred (e.g. Johnson et al., 2017, 2019, 2021b). The increasing occurrence and/or duration of growth interruptions with age is part of the reason for the commonly observed reduction in amplitude of  $\delta^{18}\text{O}$  profiles through ontogeny, but general slowing of growth (and consequent greater time averaging within samples) is also contributory (Goodwin et al., 2003; Ivany et al., 2003). Increasing sample resolution can potentially offset this effect (Schöne, 2008), but the most accurate indication of seasonal temperature variation is likely to be obtained from early ontogenetic data (Goodwin et al., 2003; Ivany et al., 2003). An exception to this rule is provided by *Magallana* (formerly *Crassostrea*) *gigas*, which exhibits substantial oxygen isotope disequilibrium in early ontogeny (Huyghe et al., 2020, 2022).

A problem as important as growth cessation/reduction for the inference of seasonal temperature range is the choice of equation relating temperature to water and shell  $\delta^{18}\text{O}$ . Various equations exist for both aragonite and calcite, and for the same range in shell  $\delta^{18}\text{O}$ , these yield different temperature ranges. Thus for a water value of 0.0‰ and summer and winter shell values of 0.0‰ and +2.0‰, respectively, the widely employed aragonite equation of Grossman and Ku (1986) yields seasonal temperatures of 19.4 and 10.7 °C – i.e. a seasonal range of 8.7 °C. However, for the same  $\delta^{18}\text{O}$  values the *Glycymeris glycymeris*-specific aragonite equation of Royer et al. (2013) yields seasonal temperatures of 17.4 and 12.1 °C – i.e. a seasonal range of only 5.3 °C. Since both equations are linear, like the LL (low-light) calcite equation of Bemis et al. (1998), used by Johnson et al. (2021b), neither the absolute values specifying a summer–winter difference of 2.0‰ in shell  $\delta^{18}\text{O}$  nor the value of water  $\delta^{18}\text{O}$  affect the calculated seasonal temperature range. However, the non-linear calcite equations of O’Neil et al. (1969; as reformulated by Shackleton et al., 1974) and Kim and O’Neil (1997) not only yield different temperature ranges for a given range in shell  $\delta^{18}\text{O}$ , but the temperature range in each case varies with the absolute shell values concerned and with water  $\delta^{18}\text{O}$ . Thus for a water value of 0.0‰ and summer and winter shell values of 0.0‰ and +2.0‰, respectively, the calcite equation of O’Neil et al. (1969) yields a seasonal temperature range of 8.2 °C (summer 15.7 °C, winter 7.5 °C) and that of Kim and O’Neil (1997) a seasonal temperature range of 8.9 °C (summer 13.7 °C, winter 4.8 °C), but for a water value of +0.4‰ and summer and winter shell values of +1.5‰ and +3.5‰ (i.e. the same 2.0‰ range but at higher absolute values), the

equation of O’Neil et al. (1969) yields a seasonal temperature range of 7.8 °C (summer 11.1 °C, winter 3.3 °C) and that of Kim and O’Neil (1997) a seasonal temperature range of 8.6 °C (summer 8.8 °C, winter 0.2 °C). The differences in seasonal temperature range due to different water  $\delta^{18}\text{O}$  and absolute shell  $\delta^{18}\text{O}$  values are not great, but the differences due to different equations are fairly significant for calcite (up to almost 1 °C for the water and shell  $\delta^{18}\text{O}$  values specified above) and quite major for aragonite (over 3 °C). Clearly, therefore, the choice of equation must be given careful consideration.

Modelling (e.g. Williams et al., 2009) and carbonate clumped isotope ( $\Delta_{47}$ ) analysis (e.g. Briard et al., 2020; Caldarescu et al., 2021) are techniques that have been used to constrain water  $\delta^{18}\text{O}$ . The studies cited in relation to the latter approach employ it to resolve seasonal fluctuations, and de Winter et al. (2021) discuss the best sampling strategy to achieve this end. In nearshore settings affected by major seasonal influxes of freshwater (normally isotopically light) and which exhibit concomitant reductions in salinity, variation in water  $\delta^{18}\text{O}$  may be quite high. Lloyd (1964) documented change of more than 1‰ over a few months in part of Florida Bay, and Ivany et al. (2004) inferred seasonal variation of 2.5‰ in an Eocene nearshore setting in the south-eastern USA. However, in more offshore settings the effects of freshwater influx are much less. Thus in the modern North Sea seasonal variation in salinity is in most places only 0.25 PSU (Howarth et al., 1993), which translates to a seasonal variation in water  $\delta^{18}\text{O}$  of just 0.07‰ using the salinity–water  $\delta^{18}\text{O}$  relationship for the North Sea of Harwood et al. (2008). Within a few tens of kilometres of the mouth of the Rhine seasonal variation in salinity rises to 0.75 PSU, and hence calculated variation in water  $\delta^{18}\text{O}$  rises to 0.21‰. At 20–30 m depth in the eastern part of the central North Sea, Schöne and Fiebig (2009) identified variation in salinity of up to 2 PSU in certain years, which translates to a variation in water  $\delta^{18}\text{O}$  of 0.55‰. If minimum and maximum water  $\delta^{18}\text{O}$  values differing by this amount coincided, respectively, with the times of maximum and minimum water temperature, it would increase the temperature range calculated from shell  $\delta^{18}\text{O}$  assuming constant water  $\delta^{18}\text{O}$  by an amount in the order of 2.6 °C (figure for calcite using the LL equation mentioned above). However, the data of Schöne and Fiebig (2009) provide no evidence of a negative correlation between salinity/water  $\delta^{18}\text{O}$  and temperature, and near the eastern shore of the central North Sea there is a very strong positive correlation between water  $\delta^{18}\text{O}$  and temperature over the seasonal cycle (Ullmann et al., 2010; de Winter et al., 2021). This presumably reflects relatively high evaporation in summer, combined with relatively low freshwater input, a common pattern in midlatitude settings and one suggesting that seasonal variation in shell  $\delta^{18}\text{O}$  of marine organisms at midlatitudes is more likely to be damped than enhanced by variation in water  $\delta^{18}\text{O}$ .

Even if there were a negative correlation between water  $\delta^{18}\text{O}$  and temperature, it would be confined to nearshore waters (more susceptible to freshwater influx); hence the effect on calculated temperature range could be mitigated by the use of offshore shells. This approach introduces the possibility of underestimation of the surface range as a result of life positions below the summer thermocline (typically at 25–30 m depth in shelf settings). However, shells from sub-thermocline settings may be recognized from the associated sediments and biota and, in the case of the scallop *Aequipecten opercularis*, from microgrowth-increment patterns (Johnson et al., 2009, 2021b; Fig. 1).

While  $\delta^{18}\text{O}$  sclerochronology is potentially informative about seasonality, it should be clear from the foregoing that results from the technique need to be interpreted carefully. The reliability of the information is of course also dependent on preservation of the original shell  $\delta^{18}\text{O}$  signature. Ivany and Judd (2022) provide a perspective on the issues considered above and in addition present a mathematical approach to reconstructing seasonality from the  $\delta^{18}\text{O}$  profiles of organisms whose growth rate is not uniform. This is, however, dependent on a strictly sinusoidal pattern of temperature variation over the year, which, as Ivany and Judd (2022) note, cannot be assumed in sub-thermocline situations (i.e. in the likely setting of some of the shells considered herein; see Sects. 3 and 5.3)

### 3 Setting and material

In the Pliocene the marine area of the SNSB was somewhat greater than now (Fig. 2), partly due to higher global sea level and partly to subsequent regional uplift (Westaway et al., 2002). Onshore marine deposits exist to the west in eastern England, and to the east in Belgium and the Netherlands, those in the last two countries passing eastwards into essentially fluvial non-marine deposits of the proto-Rhine–Meuse–Scheldt River system (Louwye et al., 2020; Munsterman et al., 2020). The Eridanos River system, draining the Baltic area, had its exit into the SNSB in the area of the present German Bight, some 400 km north-east of the proto-Rhine–Meuse–Scheldt exit (Gibbard and Lewin, 2016). While at certain times a link may have existed between the SNSB and the Channel Basin during the Pliocene (either at the present position or across southern England; Funnell, 1996; Westaway et al., 2002; van Vliet-Lanoë et al., 2002; Gibbard and Lewin, 2016), at others the basins were separated by the Weald–Artois land bridge, as shown in Fig. 2. Water depth in the southern North Sea is now less than 40 m in most places but seismic stratigraphy indicates that it was greater in the Pliocene, at least in areas of low sediment accumulation (Overeem et al., 2001).

In eastern England there is a large stratigraphic gap between the Zanclean Coralline Crag Formation and the late Piacenzian basal unit (“Walton Crag”) of the Red Crag For-

mation, but the Piacenzian is better recorded in northern Belgium by the Lillo Formation and in the south-west Netherlands by the Oosterhout Formation (Fig. 3). The last two formations essentially comprise marine sands, the Oosterhout Formation at Ouwkerk (Zeeland) probably having been deposited in deeper water than the Lillo Formation at Antwerp from the evidence of fish otoliths (Gaemers and Schwarzahns, 1973) and a position farther from the inferred shoreline (Fig. 2). Nevertheless, Slupik et al. (2007) inferred a depth of deposition above storm wave base for most of the Oosterhout Formation at Schelphoek, 15 km north-west of Ouwkerk. In the Antwerp area depth estimates based on the fauna have varied between authors according to the group studied, most of them hardly taking into account the marked variation in sediment and sedimentary structures within members of the Lillo Formation (see Deckers et al., 2020, Figs. 4–6). According to Gaemers (1975), the otolith assemblage indicates a depth of at least 10–20 m for the “Kallo Sands” (Lillo Formation, Oorderen Member; Marquet and Herman, 2009) but less than 10 m for the overlying Kruisschans Member. This indication of upward shallowing is supported by assemblage evidence from dinocysts (Louwye et al., 2004; De Schepper et al., 2009), Foraminifera (Laga, 1972), and bivalves (Marquet, 2004), but statistical data from the last group suggest greater absolute depths: 35–45 m for the Oorderen Member and 15–55 m for the Kruisschans Member by the common overlap in depth range of extant species; 40–50 m for the former and 20–50 m for the latter by the medial depth of extant species. The articulated preservation of the semi-infaunal bivalve *Atrina fragilis*, locally in life position, within the Oorderen Member (Marquet and Herman, 2009) is difficult to reconcile with the 10–20 m minimum depth estimate of Gaemers (1975), since specimens would have been subject to fair-weather processes after death. It is more likely that they lived at the depth suggested by Marquet (2004) and were killed by rapid burial (and permanently interred) in storms. A somewhat greater depth still was inferred from the bivalve assemblage of the underlying Luchtbal Member: 40–50 m by “common overlap”; 40–60 m by “medial depth”. The low diversity of the bivalve fauna of the Merksem Member (overlying the Kruisschans Member) precluded the same statistical treatment, but Marquet and Herman (2009) inferred from this impoverishment a depth of less than 15 m, an estimate consistent with the foraminiferal assemblage (Laga, 1972) and the high proportion of terrestrial palynomorphs (De Schepper et al., 2009).

Dinocyst assemblages indicate surface temperatures within the warm temperate range (but possibly only with respect to summer; Sect. 1) during the deposition of most of the Oorderen Member but punctuated by cool intervals and preceded by continuously cool conditions during the deposition of the Luchtbal Member (De Schepper et al., 2009). The dinocysts of the Kruisschans and Merksem members mainly indicate a continuation of the warm conditions of the Oorderen Member but provide a few hints of cooling

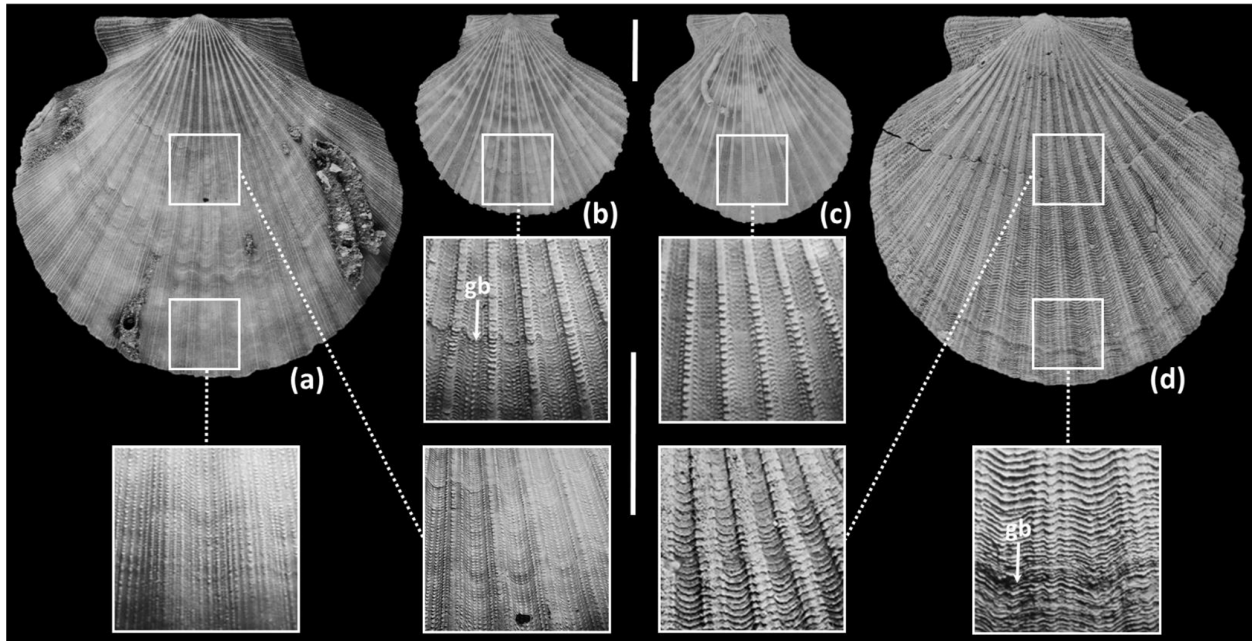


**Figure 1.** Pictorial demonstration of microgrowth-increment patterns in left valves of *Aequipecten opercularis*. **(a)** Typical supra-thermocline specimen (mesotidal setting, 23 m depth, La Coruña, Galicia, Spain) showing small increments early and late in ontogeny. **(b, c)** Typical sub-thermocline specimens **(b)** microtidal setting, 50 m depth, Gulf of Tunis, Tunisia; **(c)** microtidal setting, 38 m depth, Adriatic Sea, Pula, Croatia) showing large increments early in ontogeny. **(d)** Inferred sub-thermocline specimen (Ramsholt Member, Coralline Crag Formation, Broom Pit, Suffolk, UK) showing large increments early in ontogeny and a transition from large to small increments late in ontogeny. Scale bars of 10 mm for whole-shell images (upper) and enlargements (lower). Major growth breaks (gb) identified in enlargements of **(b, d)**. **(a)** University of Derby, Geological Collections (UD) 53424; **(b)** National Museum of Natural History, Paris, IM-2008-1542 (one of seven specimens in this lot); **(c)** UD 53423 (one of 48 specimens in this lot, coded S3A29); **(d)** UD 53425. See Johnson et al. (2009, 2021b) for numerical data and discussion of microgrowth-increment patterns in *A. opercularis*. Modern supra-thermocline specimens show a difference of < 0.3 mm between the maximum and minimum values of smoothed increment-height profiles, while the majority of sub-thermocline specimens show a difference of > 0.3 mm.

(Louwye et al., 2004; De Schepper et al., 2009). Other evidence of this is provided by bivalves, fish, and pollen (Hacquart, 1960; Vandenberghe et al., 2000; Marquet, 2005), and Wood et al. (1993) determined a 5–6 °C decrease in summer surface temperature from the ostracods of a contemporaneous part of the Oosterhout Formation.

Previous sclerochronological investigation of late Pliocene temperatures in Belgium and the Netherlands focussed on the Oorderen Member and an equivalent horizon in the Oosterhout Formation and was restricted to  $\delta^{18}\text{O}$  data from two bivalve species: *Aequipecten opercularis* and *Atrina fragilis* (Valentine et al., 2011). Here we supplement the existing  $\delta^{18}\text{O}$  data from *A. opercularis* with microgrowth-increment data from the same specimens to gain an insight into their hydrographic setting (sub- or supra-thermocline), and we also supply  $\delta^{18}\text{O}$  data from two further bivalve species (*Arctica islandica* and *Pygocardia rustica*) from the Oorderen Member and another (*Glycymeris radiolyrata*) from the Luchtbal Member. In addition, we provide *A. opercularis* data from the Luchtbal Member and horizons equivalent to the Luchtbal and Merksem members in the Oosterhout Formation. Values for  $\delta^{13}\text{C}$  (obtained alongside  $\delta^{18}\text{O}$ ) are reported

for all species. Details of the provenance of the specimens are given in Table 1, together with alphanumeric codes (AO: *A. opercularis*; AI: *A. islandica*; PR: *P. rustica*; GR: *G. radiolyrata*) and sundry basic descriptive information. Note that the five specimens from the Oorderen Member sensu stricto come from the *Atrina fragilis* bed, a horizon with the warm temperate dinocyst assemblage found at most levels in the member. Illustrations of species other than *A. opercularis* (Fig. 1) are provided in Fig. 4. Most, if not all, of the material from the Lillo Formation was obtained from temporary exposures created during harbour works in the Antwerp area, while all the material from the Oosterhout Formation was obtained from a borehole (Rijkswaterstaat-Deltadienst, afdeling Waterhuishouding, 42H19-4/42H0039) at Ouwerkerk, Zeeland. Interpretation of positions (depths) within the Ouwerkerk borehole in terms of members within the Lillo Formation follows Gaemers and Schwarzans (1973) except in the case of AO8, for which we have accepted the opinion of Frank Wesselingh (in Valentine et al., 2011) that the position is equivalent to the Oorderen Member. Gaemers and Schwarzans (1973) considered that strata of this age (Kallo Sands) were missing at Ouwerkerk, but they appear to be

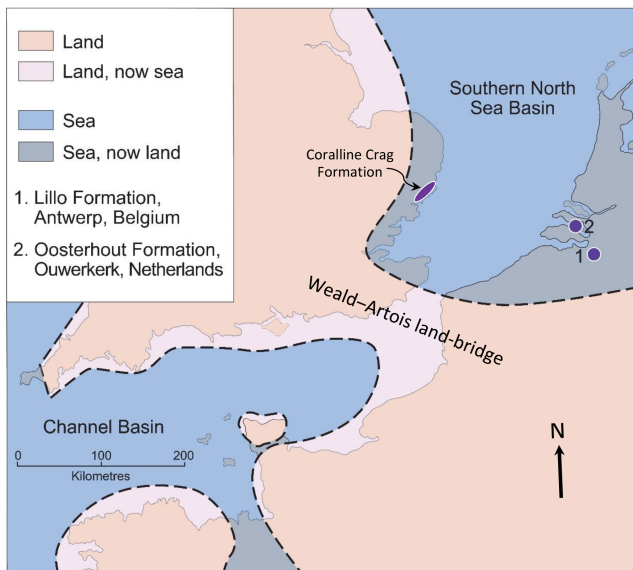


**Figure 2.** Pliocene palaeogeography in the vicinity of the SNSB, the location of sites in the Lillo (1) and Oosterhout (2) formations, from which shells were obtained, and the area of onshore outcrop of the Coralline Crag Formation in eastern England (the partly Pleistocene Red Crag Formation occurs over a larger area). Adapted from Valentine et al. (2011, Fig. 1), itself based on Murray (1992, map NG1).

well represented at Schelphoek, only 15 km away (Slupik et al., 2007).

According to the latest chronostratigraphy (Fig. 3), the material investigated is largely or entirely Piacenzian (3.60–2.59 Ma) in age, the oldest (from the Luchtbal Member of the Lillo Formation) being possibly as old as 3.71 Ma (latest Zanclean) and the youngest (from horizons in the Oosterhout Formation equivalent to the Merkssem Member of the Lillo Formation) being no younger than 2.76 Ma (De Schepper et al., 2009). The MPWP is probably represented by material from the Oorderen Member and the equivalent level in the Oosterhout Formation (Valentine et al., 2011). The Luchtbal and Oorderen members are separated by an unconformity interpreted by De Schepper et al. (2009) as a product of the sea-level fall associated with Marine Isotope Stage (MIS) M2 (ca. 3.3 Ma), which marks a glacial episode. The Luchtbal Member was therefore probably deposited before MIS M2 under interglacial conditions.

All the specimens come from stratigraphic intervals with a fully marine associated biota (e.g. Marquet, 2002, 2005; Gaemers and Schwarzahans, 1973), in conformity with modern occurrences in the case of the extant species *A. opercularis* and *A. islandica* (Tebble, 1976) and other fossil occurrences in the case of the extinct species *P. rustica* and *G. radiolyrata* (Norton, 1975; Buchardt and Simonarson, 2003; Marquet, 2002, 2005). Investigation of specimens of *A. islandica*, *P. rustica*, and *G. radiolyrata* added information

from infaunal, slow-growing taxa to that derived from fast-growing, epifaunal *A. opercularis*, hence serving to mitigate any “ecological” bias in the results. We could not sample as many specimens of the infaunal, slow-growing species as of *A. opercularis* due to the limited availability of material (perforce from museums, in the lack of extant stratal exposures in the area of study). However, we sampled multiple years in the infaunal, slow-growing species, so the combined number of seasonal cycles investigated was similar to that in *A. opercularis*. We nevertheless expected some imbalance in the data because modern examples of *Glycymeris* species, from both cool- and warm-temperate settings, show winter cessation or slowing of growth and thus supply (or would supply) underestimates of the seasonal temperature range from  $\delta^{18}\text{O}$  sclerochronology (Peharda et al., 2012, 2019a, b; Royer et al., 2013; Reynolds et al., 2017; Featherstone et al., 2020; Alexandroff et al., 2021). Various equations have been used to express the precise relationship between  $\delta^{18}\text{O}$  and temperature in modern *Glycymeris* (Royer et al., 2013; Peharda et al., 2019a, b), but species of this genus certainly exhibit something at least close to equilibrium isotopic incorporation. The same is true of *A. opercularis* (Hickson et al., 1999; Johnson et al., 2021b) and *A. islandica* (Schöne, 2013; Mette et al., 2018; Trofimova et al., 2018). Because of the similarity of  $\delta^{18}\text{O}$  values from seemingly well-preserved *P. rustica* from the Pliocene of Iceland to those from co-occurring, similarly preserved *A. islandica* (Buchardt and Simonarson, 2003) it is reasonable to assume equilibrium fractionation in the former (extinct) species. The specimens analysed showed no physical signs of alteration, and they are unlikely to have been heated by more than 10 °C through burial as the thickness of overlying sediments was probably never much more than 100 m (the depth below the present surface of the lowermost shell from the Ouwerkerk borehole). Examples of both calcitic *A. opercularis* (including AO7 herein) and aragonitic *A. fragilis* from the Lillo Formation were shown by Valentine et al. (2011) to exhibit the original shell microstructure. Similarly good preservation has been demonstrated in a variety of calcitic and aragonitic species from the slightly earlier Ramsholt Member of the Coralline Crag Formation in eastern England (Johnson et al., 2009; Vignols et al., 2019). We therefore considered it reasonable to proceed with isotopic analysis of our material (both calcitic and aragonitic; see Sect. 4 and Table 1) without detailed investigation of its preservation. Moon et al. (2021) have recently shown that good mineralogical and microstructural preservation does not necessarily guarantee good preservation of original shell  $\delta^{18}\text{O}$ . They heated shell material to 200 °C and identified consistent negative shifts in  $\delta^{18}\text{O}$  (1.5 ‰ after 2 weeks at this temperature) over an annual cycle but no significant mineralogical or microstructural changes. As our specimens experienced only minimal heating through burial, similar alteration of shell  $\delta^{18}\text{O}$  is unlikely.

**Table 1.** Basic information for the investigated specimens (all single valves). Order stratigraphic within formations (by member, then by borehole depth or bed, with entries for the Oosterhout Formation inserted immediately above those, if any, for the equivalent member in the Lillo Formation). Entries in square brackets are interpretations (see footnotes). Latitudes and longitudes are for the location indicated in the adjacent column and do not necessarily specify the exact place of collection (see Fig. 2 for the positions of Ouwkerk and Antwerp). UD: University of Derby, Geological Collections; IRSNB: Royal Belgian Institute of Natural Sciences, Brussels (MSNB was used for specimens discussed in Valentine et al., 2011).

| Formation  | Member or equivalent (in quotes) | Borehole depth (b-d) or bed     | Location                   | Latitude, longitude | Genus and species              | Repository and number   | Code herein | Valve height (mm) | General physical condition | Mineralogy of sampled layer | Number of isotope samples |
|------------|----------------------------------|---------------------------------|----------------------------|---------------------|--------------------------------|-------------------------|-------------|-------------------|----------------------------|-----------------------------|---------------------------|
| Oosterhout | “Merksem”                        | b-d: 89.75–91 m                 | Ouwkerk                    | 51.626° N, 3.983° E | <i>Aequipecten opercularis</i> | UD 53362                | AO10        | 56                | Incomplete                 | Calcite                     | 42                        |
| Oosterhout | “Merksem”                        | b-d: 93.5–94.5 m                | Ouwkerk                    | 51.626° N, 3.983° E | <i>Aequipecten opercularis</i> | UD 53363                | AO9         | 46                | Incomplete                 | Calcite                     | 30                        |
| Oosterhout | “Oorderen”                       | b-d: 98.5–99.5 m                | Ouwkerk                    | 51.626° N, 3.983° E | <i>Aequipecten opercularis</i> | UD 53347                | AO8         | 34                | Incomplete, abraded        | Calcite                     | 31                        |
| Lillo      | Oorderen                         | <i>Atrina fragilis</i> bed      | Vrasenedok, Kallo, Antwerp | 51.263° N, 4.238° E | <i>Aequipecten opercularis</i> | IRSNB Invert-29710-10   | AO7         | 42                | Complete                   | Calcite                     | 31                        |
| Lillo      | Oorderen                         | <i>Atrina fragilis</i> bed      | Vrasenedok, Kallo, Antwerp | 51.263° N, 4.238° E | <i>Aequipecten opercularis</i> | IRSNB Invert-29710-09   | AO6         | 51                | Complete                   | Calcite                     | 39                        |
| Lillo      | Oorderen                         | Base <i>Atrina fragilis</i> bed | Deugancdkok, Doel, Antwerp | 51.291° N, 4.257° E | <i>Aequipecten opercularis</i> | IRSNB Invert-D2-8       | AO5         | 31                | Complete                   | Calcite                     | 23                        |
| Lillo      | Oorderen                         | <i>Atrina fragilis</i> bed      | Vrasenedok, Kallo, Antwerp | 51.263° N, 4.238° E | <i>Pygocardia rustica</i>      | IRSNB Invert-29710-04   | PR          | 62                | Complete                   | Aragonite                   | 37                        |
| Lillo      | Oorderen                         | <i>Atrina fragilis</i> bed      | [Antwerp] <sup>a</sup>     | 51.217° N, 4.421° E | <i>Arctica islandica</i>       | IRSNB Invert-18201-01   | AI          | 64                | Complete                   | Aragonite                   | 32                        |
| Oosterhout | “Luchtbal”                       | b-d: 106–107.5 m                | Ouwkerk                    | 51.626° N, 3.983° E | <i>Aequipecten opercularis</i> | UD 53364                | AO4         | 44                | Incomplete, abraded        | Calcite                     | 36                        |
| Lillo      | Luchtbal                         | <i>Palliolium gerardi</i> bed   | Deugancdkok, Doel, Antwerp | 51.291° N, 4.257° E | <i>Aequipecten opercularis</i> | IRSNB Invert-29710-13   | AO3         | 42                | Complete                   | Calcite                     | 28                        |
| Lillo      | Luchtbal                         | <i>Palliolium gerardi</i> bed   | Deugancdkok, Doel, Antwerp | 51.291° N, 4.257° E | <i>Aequipecten opercularis</i> | IRSNB Invert-29710-12   | AO2         | 47                | Complete                   | Calcite                     | 30                        |
| Lillo      | Luchtbal                         | <i>Palliolium gerardi</i> bed   | Deugancdkok, Doel, Antwerp | 51.291° N, 4.257° E | <i>Aequipecten opercularis</i> | IRSNB Invert-29710-11   | AO1         | 54                | Complete                   | Calcite                     | 28                        |
| Lillo      | Luchtbal                         | [lower bed] <sup>b</sup>        | Deugancdkok, Doel, Antwerp | 51.291° N, 4.257° E | <i>Glycymeris radiolyrata</i>  | IRSNB 7698              | GR2         | 77                | Broken in storage          | Aragonite                   | 74                        |
| Lillo      | Luchtbal                         | [lower bed] <sup>b</sup>        | Deugancdkok, Doel, Antwerp | 51.291° N, 4.257° E | <i>Glycymeris radiolyrata</i>  | IRSNB Invert-29710-0062 | GR1         | 92                | Broken in storage          | Aragonite                   | 42                        |

<sup>a</sup> No specific location indicated within Belgium but highly likely to be Antwerp. <sup>b</sup> Species indicated as “special” to the lower bed of the Luchtbal Member in the Deugancdkok (Marquet, 2002).

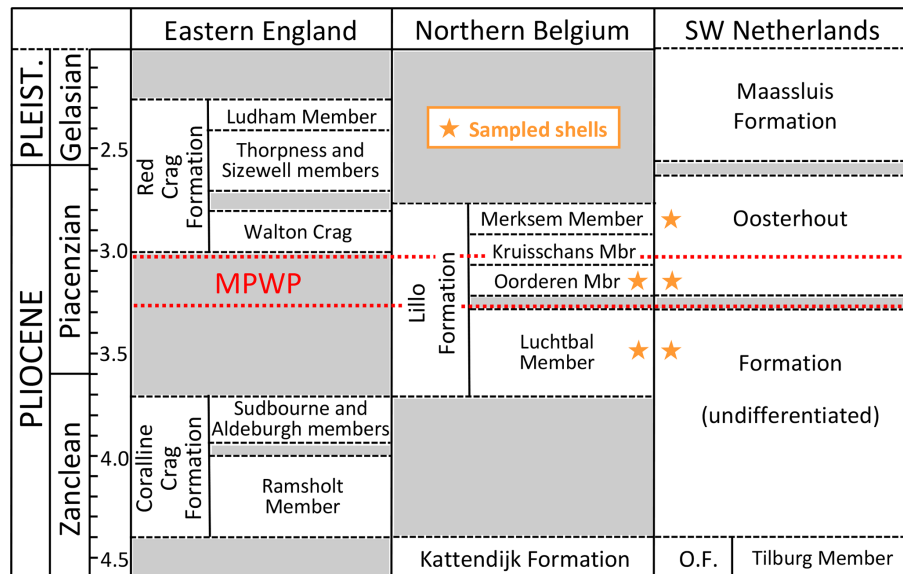


**Figure 3.** Stratigraphy and correlation of marine mid–late Pliocene and early Pleistocene units of the southern North Sea basin, with the general stratigraphic positions of shells sampled for the present study (specific positions in Table 1). Age (Ma) of the Red Crag Formation and constituent members (including the unofficial Walton Crag unit) according to Wood et al. (2009); of the Coralline Crag, Kattendijk and Lillo formations and constituent members according to De Schepper et al. (2009) and Louwye and De Schepper (2010); and of the Oosterhout (O.F.) and Maassluis formations according to Dearing Crampton-Flood et al. (2020) and Wesselingh et al. (2020). An additional small hiatus, of uncertain age, is present in the lower part of the Oosterhout Formation (Dearing Crampton-Flood et al., 2020). The Maassluis Formation includes a number of non-marine horizons (Slupik et al., 2007). Names of Lillo Formation members are in accordance with recent practice (Louwye et al., 2020; Wesselingh et al., 2020), omitting “Sand”/“Sands”, as included by previous authors. Wesselingh et al. (2020) found evidence of an additional layer (Broechem Unit) between the Kattendijk Formation and Luchtbal Member of the Lillo Formation. De Meuter and Laga (1976) designated an additional, uppermost division of the latter formation (Zandvliet Member), but this may be no more than the decalcified top of the Merksem Member (Louwye et al., 2020). Geographic provenance of shells and the location of the Coralline Crag Formation are shown in Fig. 2. MPWP: Mid-Piacenzian Warm Period.

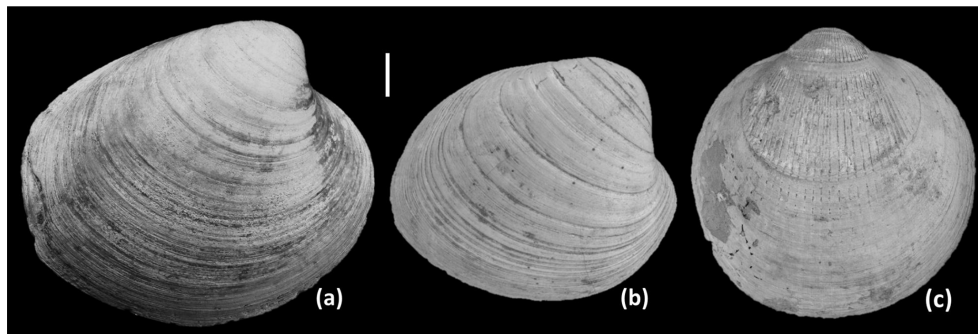


**Figure 4.** Right valves of (a) *Arctica islandica*, (b) *Pygocardia rustica*, and (c) *Glycymeris radiolyrata* from the Lillo Formation, Antwerp. (a) Probably Oorderen Member, Verrebroekdok (IRSNB 7699); (b) Oorderen Member, Verrebroekdok (IRSNB 7700); (c) Luchtbal Member, Deurganckdok (IRSNB 7701). Growth breaks are evident in all three specimens – e.g. ca. 10 major growth breaks in (b). Scale bar: 10 mm.

## 4 Methods

### 4.1 Laboratory procedures

The exterior of *A. opercularis* shells was coated with a sublimate of ammonium chloride and digitally photographed for the purpose of measuring microgrowth increments and the position of growth breaks. The coating was washed off

with tap water and the shells then underwent the further cleaning procedure adopted by Valentine et al. (2011) for removal of any surficial organic matter, in preparation for isotopic sampling of the outer shell layer from the exterior, as in other such investigations of *A. opercularis* (e.g. Hickson et al., 1999, 2000; Johnson et al., 2009, 2021b; Vignols et al., 2019). The infaunal species were sampled in

cross-section along the line of maximum growth, in accordance with universal practice for *A. islandica* (e.g. Schöne et al., 2005) and common practice for *Glycymeris* species (e.g. Royer et al., 2013). For this purpose shells were stabilized in resin before sectioning – by the partial-encasement method of Schöne et al. (2005) for *A. islandica* and *P. rustica* and the total-encasement method of Johnson et al. (2021a) for *G. radiolyrata* (fragments bonded beforehand). The use of vacuum impregnation in the latter method resulted in resin penetration into the outer part of the outer shell layer.

Extraction of isotope samples from *A. opercularis* shells was by drilling a dorsal to ventral series of shallow com-marginal grooves (depth and width < 1 mm; see Hickson et al., 1999, their Fig. 2; 2000, their Fig. 3) in the external surface, with the sample sites more closely spaced towards the ventral margin in an attempt to maintain temporal resolution in the face of declining growth rate with age. Details of the procedure are given in Johnson et al. (2019) with respect to another scallop species. Mean sample spacing for individuals – the average distance between the centres of grooves along the dorso-ventral (maximum-growth/shell-height) axis – was 0.93 (AO8)–1.35 (AO9) mm. Sampling of the infaunal species was by drilling a series of holes (depth and width < 1 mm; Fig. 5) in the outer shell layer as seen in cross-section, the curved path being located about mid-way between the external surface and the boundary between the outer and inner shell layers in *A. islandica* and *P. rustica* but somewhat closer to the latter boundary in *G. radiolyrata* to avoid resin-contaminated material (Fig. 5). Sample spacing was more constant than for *A. opercularis*, although significantly reduced late in the long series from *G. radiolyrata* GR2, again to maintain temporal resolution. Mean sample spacing for individuals – the average distance between the centres of holes, measured in terms of the difference in straight-line distance from the origin of growth – was 0.69 mm for *A. islandica*, 0.57 mm for *P. rustica*, and 0.54 mm (GR2) and 0.57 mm (GR1) for *G. radiolyrata*. Note that in these relatively convex species the straight-line distance from the origin of growth is not a measurement of shell height as normally defined (a distance from the umbo, which protrudes dorsally of the origin of growth in these forms; e.g. Fig. 5) and that the plane in which it was measured (along the line of maximum growth) arguably does not include the shell-height axis in the prosogyrate species *A. islandica* and *P. rustica* (dependent on the point at the shell margin that is regarded as ventral). The lines of measurement and the values obtained are, however, regarded as “heights” for all four species considered herein, for the sake of simplicity. The *A. opercularis* shells were relatively small (Table 1) and were sampled from near the origin of growth (dorsal margin) to a point at or close to the ventral margin (maximum sample height 53.0 mm in AO10). The shells of the infaunal species were larger (Table 1) and not sampled to the end of ontogeny (maximum sample height 54.7 mm in GR2). Furthermore, the thinness of the outer layer close to the origin

of growth meant that sampling had to start relatively far from this point (minimum sample height 15.4 mm in GR2).

The cross-sections of the infaunal species were digitally photographed for the purpose of measuring the positions of sample holes and growth breaks, as seen on the shell exterior (Fig. 4) and projected or traced (Fig. 5) into the isotope sample path. Distances from the origin of growth were determined from the images using the bespoke measuring software Panopea (© 2004 Peinl and Schöne). Panopea was also used to measure the position of growth breaks and the height of microgrowth increments in the shell-exterior images of *A. opercularis* (see Fig. 1). As in the case of isotope sample positions, measurements were made along the dorso-ventral axis or (where this was impossible due to abrasion or encrustation) lateral to this line, the measurements then being mathematically adjusted as described by Johnson et al. (2019) to correspond to ones made along the dorso-ventral axis. All the microgrowth-increment measurements were made by the same person (Annemarie M. Valentine), thus assuring a reasonably uniform approach given the subjective element in increment identification (Johnson et al., 2021b). Growth breaks were classified as major (incorporating “moderate”) or minor in all species dependent on their external prominence (see Figs. 1, 4).

Samples (typically 50–100 µg) were analysed for their stable oxygen and carbon isotope composition (given as  $\delta^{18}\text{O}$  and  $\delta^{13}\text{C}$ ) at the stable isotope facility, British Geological Survey, Keyworth, UK (*A. opercularis*, *A. islandica*, *P. rustica*), and the Institute of Geosciences, University of Mainz, Germany (*G. radiolyrata*). At Keyworth, samples were analysed using an Isoprime dual-inlet mass spectrometer coupled to a Multiprep system; powder samples were dissolved with concentrated phosphoric acid in borosilicate Wheaton vials at 90 °C. At Mainz, samples were analysed using a Thermo Finnigan MAT 253 continuous-flow isotope ratio mass spectrometer coupled to a Gasbench II; powder samples were dissolved with water-free phosphoric acid in helium-flushed borosilicate exetainers at 72 °C. Both laboratories calculated  $\delta^{13}\text{C}$  and  $\delta^{18}\text{O}$  against VPDB and calibrated data against NBS-19 (preferred values: +1.95 ‰ for  $\delta^{13}\text{C}$ , –2.20 ‰ for  $\delta^{18}\text{O}$ ) and their own Carrara Marble standard (Keyworth: +2.00 ‰ for  $\delta^{13}\text{C}$ , –1.73 ‰ for  $\delta^{18}\text{O}$ ; Mainz: +2.01 ‰ for  $\delta^{13}\text{C}$ , –1.91 ‰ for  $\delta^{18}\text{O}$ ). Values were consistently within  $\pm 0.05$  ‰ of the values for  $\delta^{18}\text{O}$  and  $\delta^{13}\text{C}$  in NBS-19. This confirms the comparability of results from each laboratory established in earlier work (Johnson et al., 2019). Note that  $\delta^{18}\text{O}$  of shell aragonite was not corrected for different acid-fractionation factors of aragonite and calcite (for further explanation, see Füllenbach et al., 2015).

#### 4.2 Calculation of temperatures

In previous work on late Pliocene bivalves from Belgium and the Netherlands, minimum and maximum estimates of global average seawater  $\delta^{18}\text{O}$  (–0.5 ‰ and –0.2 ‰) and minimum

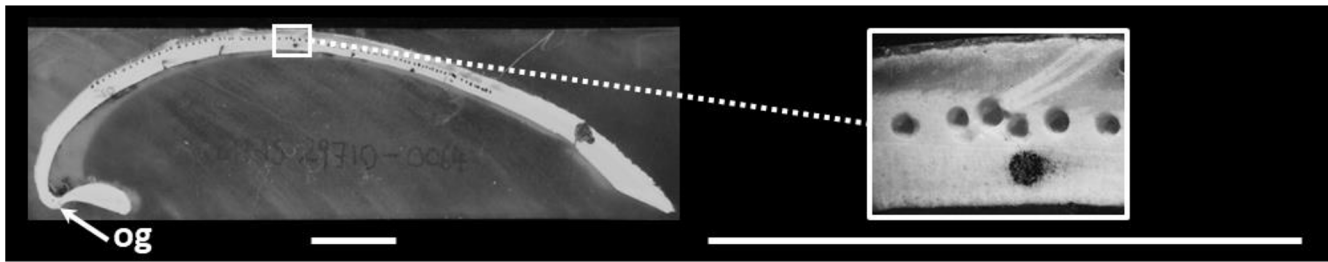


**Figure 5.** Cross-section of *Glycymeris radiolyrata* specimen GR2 showing the origin of growth (og), position of sample holes (relatively far from the external surface in this species to avoid the darker, resin-contaminated material) and a major growth break (pale diagonal band in enlargement) at shell height 35.4 mm. Scale bars: 10 mm. Black spot in enlargement is a marker to assist sample numbering.

and maximum modelled values for the early Pliocene in the western part of the SNSB (+0.1‰ and +0.5‰), all adjusted downwards by 0.1‰ to allow for the input of isotopically light freshwater into the eastern SNSB, were used to calculate sets of temperatures from shell  $\delta^{18}\text{O}$  (Valentine et al., 2011). It seems appropriate to apply the adjusted modelled values more widely to late Pliocene material from Belgium and the Netherlands. The adjusted global values are probably unreasonably low (they supply implausibly cold temperatures of 0.1 and 1.6 °C, respectively, from AO6, a specimen from a horizon with a warm temperate dinocyst assemblage) and are not used here.

Valentine et al. (2011) employed the calcite equation of O’Neil et al. (1969) for the calculation of temperatures from *A. opercularis*, but there are grounds for thinking that this provides slightly inaccurate figures (Hickson et al., 1999; Vignols et al., 2019). The LL calcite equation of Bemis et al. (1998) seems to provide more accurate figures (i.e. for modern shells, a better fit with directly measured temperatures) and certainly yields a larger estimate for seasonal range (Johnson et al., 2021b). Both equations have therefore been employed herein to generate “minimum” and “maximum” seasonal ranges from *A. opercularis*. Note that the calcite equation of Kim and O’Neil (1997) yields an intermediate estimate, but the absolute temperatures obtained from modern *A. opercularis* are too low (Johnson et al., 2021b).

Just as there is some uncertainty as to the best equation for the calculation of temperatures from *A. opercularis* calcite, so different equations have been favoured for use with aragonitic *Glycymeris glycymeris*. Royer et al. (2013) advocated the use of a species-specific equation developed by them, while Reynolds et al. (2017) provide grounds for using the general aragonite equation of Grossman and Ku (1986). The former yields a smaller estimate of seasonal range than the latter so again both have been employed herein in relation to *G. radiolyrata*. The equation of Grossman and Ku (1986) is generally used in relation to aragonitic *A. islandica* and supplies similar temperatures from co-occurring (also aragonitic) *P. rustica* specimens (Bucharth and Simonarson, 2003). This, and no other equation, has therefore been used herein in relation to these species. In calculating temperatures appro-

priate adjustments were made to allow for the different scales used in measurement of water (VSMOW) and shell (VPDB)  $\delta^{18}\text{O}$  values (Coplen et al., 1983; Vignols et al., 2019).

## 5 Basic results and analysis

The isotopic, microgrowth-increment, and growth-break data are shown in Figs. 6 (Luchtbal Member and equivalent) and 7 (Oorderen Member and equivalent; Merksem Member equivalent). Read top to bottom, left to right (i.e. in the alphabetical order of parts), the sequence in each figure is as in Table 1, read top to bottom. The raw data are available online (Johnson et al., 2021c).

### 5.1 $\delta^{18}\text{O}$ values and growth breaks

Apart from departures representing probable contamination or “noise” (see Fig. 6d and caption), all profiles show cyclical patterns of  $\delta^{18}\text{O}$  variation, from less than half a cycle in *A. opercularis* profiles starting near the origin of growth and terminating at a height of about 30 mm (AO8, AO5 – Fig. 7c, f, respectively) to between two and three in a profile terminating at 53 mm (AO10 – Fig. 7a) but from between two and three cycles to substantially more over smaller height intervals in *G. radiolyrata* (between three and four from 25–49 mm in GR1 – Fig. 6f; between eight and nine from 15–55 mm in GR2 – Fig. 6e) and in *P. rustica* and *A. islandica* (between two and three from 27–48 mm in each case – Fig. 7g, h, respectively). In *A. opercularis* profiles extending beyond one  $\delta^{18}\text{O}$  cycle, the amplitude commonly shows a clear ontogenetic decrease. This pattern is less pervasive and pronounced amongst the other species, and the *A. islandica* specimen shows an ontogenetic increase in amplitude. However, the lack of early ontogenetic data for comparison from these species should be noted. The maximum amplitudes from *G. radiolyrata* specimens are less than from most *A. opercularis* specimens, but those from *P. rustica* and *A. islandica* are similar to *A. opercularis*. Growth breaks, albeit sometimes only minor, are associated with (< 1 mm from the sample sites of) nearly all  $\delta^{18}\text{O}$  maxima and a few  $\delta^{18}\text{O}$  minima from *G. radiolyrata* but with none of the max-

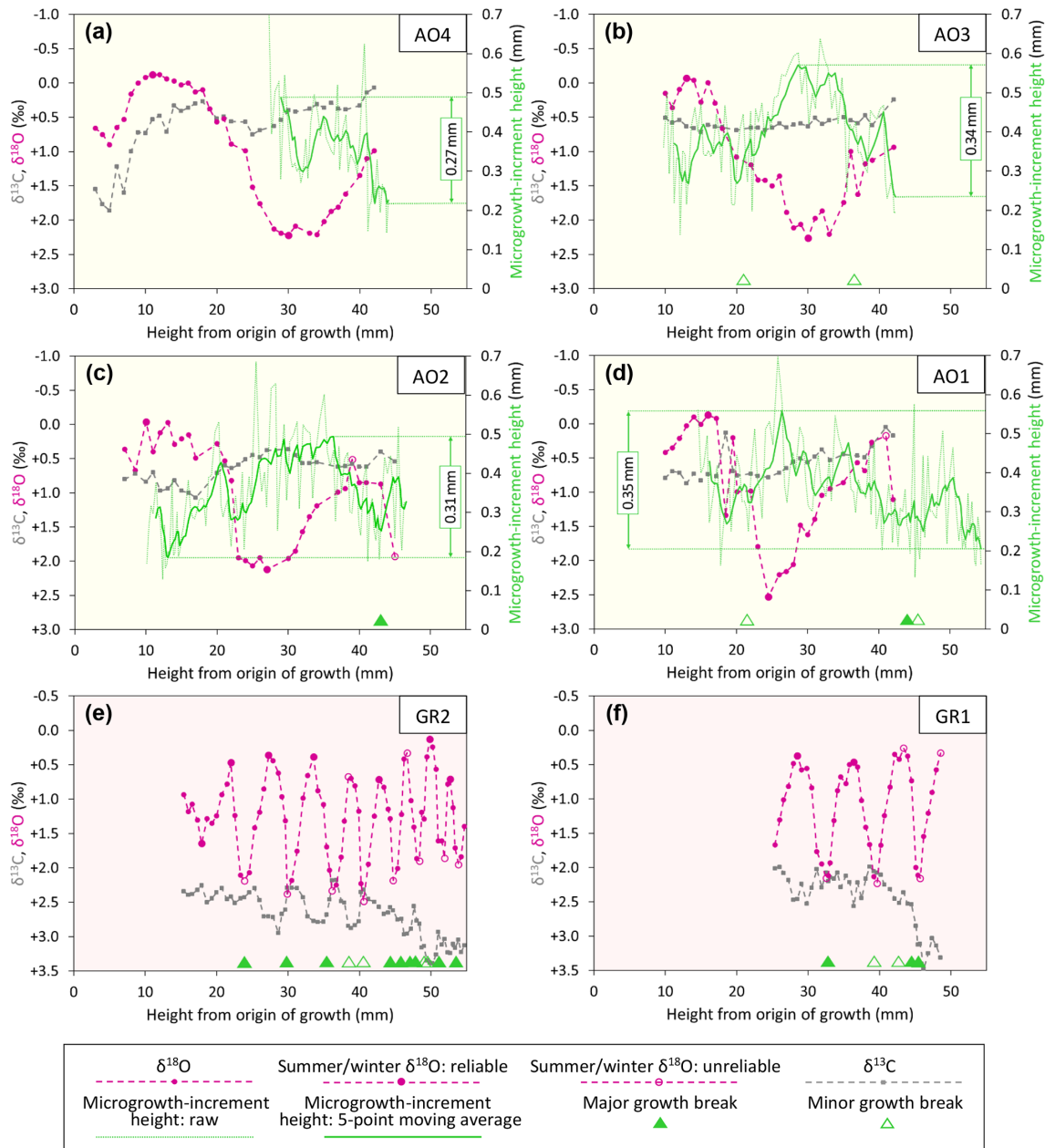


**Figure 6.** Ontogenetic profiles of  $\delta^{18}\text{O}$ ,  $\delta^{13}\text{C}$ , and microgrowth-increment height from Luchtbal Member (and equivalent) *A. opercularis* (a–d) and *G. radiolyrata* (e, f). Note that the isotopic axis has been reversed in each part such that lower values of  $\delta^{18}\text{O}$  (corresponding to higher temperatures) plot towards the top. While the axis range is 4‰ throughout, the minimum and maximum values for *A. opercularis* (calcitic; pale yellow background) have been set 0.5‰ lower than for *G. radiolyrata* (aragonitic; pale pink background) to facilitate comparison, given the different fractionation factors applying for  $\delta^{18}\text{O}$  (Kim et al., 2007). The criteria for recognition of reliable and unreliable summer and winter  $\delta^{18}\text{O}$  values are given in Sect. 6.1.1. The fairly large single-point  $\delta^{18}\text{O}$  excursion at height 18.5 mm in (d) is matched by a negative one in  $\delta^{13}\text{C}$  and probably reflects contamination. Smaller interruptions of the large-scale cyclical pattern of  $\delta^{18}\text{O}$  variation in this and other profiles represent “noise” (unexplained variability).

ima or minima from *A. opercularis*. Growth breaks are associated with two of the three maxima and two of the three minima from the *A. islandica* specimen and with two of the three minima from the *P. rustica* specimen.

Taking the  $\delta^{18}\text{O}$  cycles to reflect seasonal temperature variation and hence intervals of 1 year, the much smaller number over a given height interval from *A. opercularis* confirms that this species grew a great deal faster than the others (more than twice as fast as *A. islandica* and *P. rustica* and

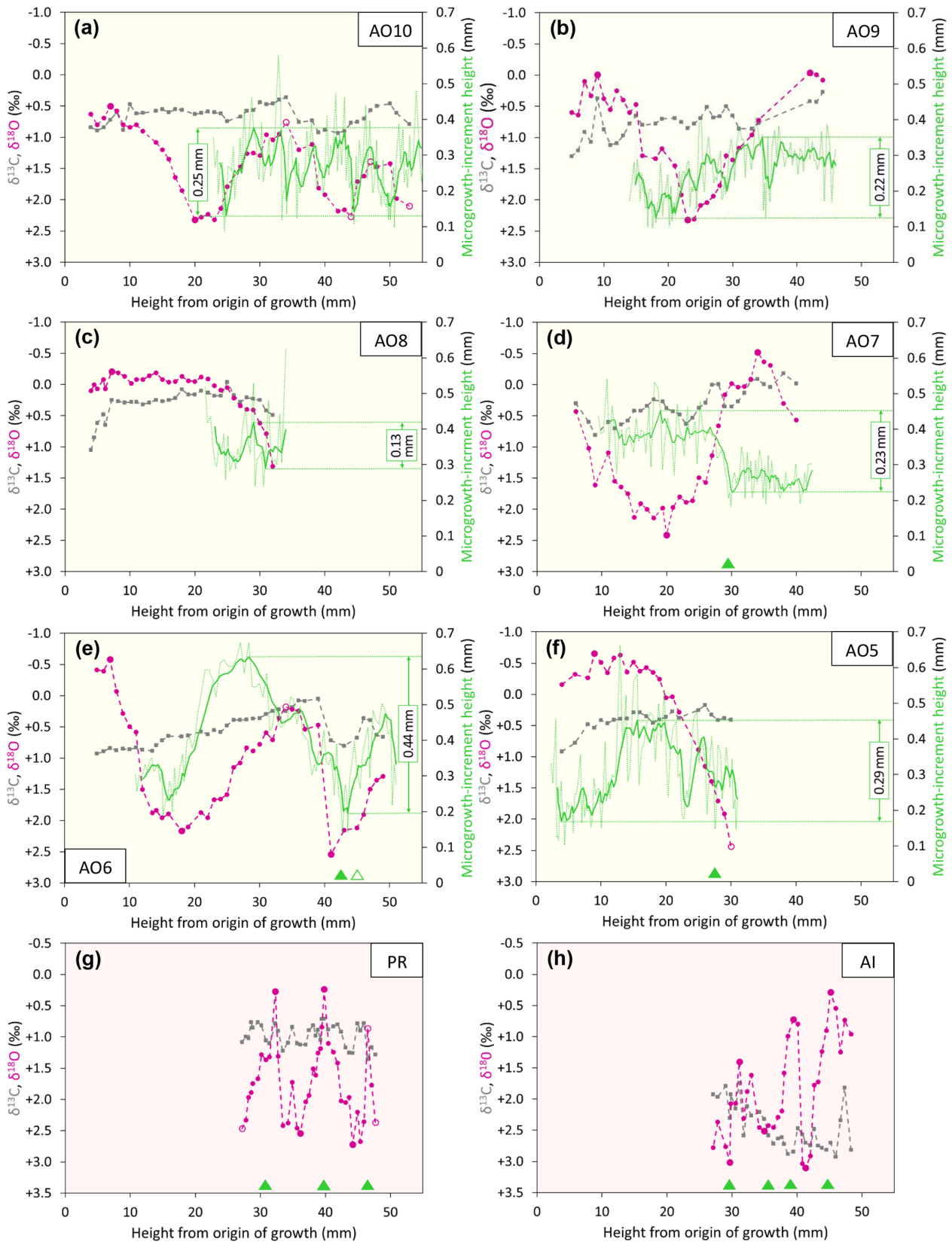


**Figure 7.** Isotopic, microgrowth-increment, and growth-break data from Merksem-equivalent *A. opercularis* (a, b) and Oorderen Member (and equivalent) *A. opercularis* (c–f), *P. rustica* (g), and *A. islandica* (h). Format and symbols as in Fig. 6.

3 to 5 times faster than *G. radiolyrata*). In *A. opercularis* profiles spanning 2 or more years (AO10, AO6 – Fig. 7a, e, respectively), there is an ontogenetic decrease in wavelength as well as amplitude – i.e. growth was fastest in early ontogeny. Ontogenetic decline in growth rate has been widely documented in *A. opercularis* from both  $\delta^{18}\text{O}$  and other evidence (e.g. Johnson et al., 2021b), and in the present instances (in which  $\delta^{18}\text{O}$  maxima and minima are not associated with growth breaks) the ontogenetic decrease in amplitude of  $\delta^{18}\text{O}$  cycles is probably a consequence of the general slowing of growth with age, leading to time averaging in samples. Whatever the explanation, seasonal temperature variation is likely to be most faithfully reflected by the first  $\delta^{18}\text{O}$  cycle in *A. opercularis* profiles. The profiles from *G. radiolyrata*, *P. rustica*, and *A. islandica* undoubtedly omit several early ontogenetic cycles and given the short wavelength of the later cycles represented, it may be that the amplitude of these is reduced by time averaging, as inferred in *A. opercularis*. Even if the closer spacing of samples from *G. radiolyrata*, *P. rustica*, and *A. islandica* may have been sufficient in principle for the resolution of seasonal  $\delta^{18}\text{O}$  extremes, the association of growth breaks with maxima, minima, or both suggests that some recorded extremes are not representative of the most extreme temperatures experienced by the organism in the season concerned – i.e.  $\delta^{18}\text{O}$  variation may not fully reflect seasonal temperature variation.

## 5.2 $\delta^{13}\text{C}$ values

Compared to  $\delta^{18}\text{O}$  values from the same specimen,  $\delta^{13}\text{C}$  values generally show much less variation, particularly within the span of  $\delta^{18}\text{O}$  cycles. Nevertheless, in some specimens there are intervals exhibiting covariation between  $\delta^{13}\text{C}$  and  $\delta^{18}\text{O}$ : moderate–strong positive covariation in AO10 (Fig. 7a), AO6 (Fig. 7e), and PR (Fig. 7g) between shell heights 25 and 53 mm ( $r^2 = 0.61$ ), 18 and 46 mm ( $r^2 = 0.84$ ), and 31 and 46 mm ( $r^2 = 0.34$ ), respectively; moderate–strong negative covariation in GR2 (Fig. 6e) and GR1 (Fig. 6f) between shell heights 25 and 43 mm ( $r^2 = 0.68$ ) and 26 and 42 mm ( $r^2 = 0.40$ ), respectively. However, the general picture is of fluctuations (if any) in  $\delta^{13}\text{C}$  that are independent of  $\delta^{18}\text{O}$ . The *A. opercularis* specimens show a marginal to clear overall decrease in  $\delta^{13}\text{C}$  through ontogeny, while the *P. rustica* specimen shows little change and the *A. islandica* and *G. radiolyrata* specimens show clear overall increases. The mean values from the *A. opercularis* specimens are very similar – from  $+0.31 \pm 0.22\text{‰}$  ( $\pm 1\sigma$ ) in AO8 to  $+0.77 \pm 0.24\text{‰}$  in AO9 – and comparable to the mean from the *P. rustica* specimen ( $+0.98 \pm 0.18\text{‰}$ ) but much lower than the means from the *A. islandica* ( $+2.44 \pm 0.35\text{‰}$ ) and *G. radiolyrata* (GR1,  $+2.42 \pm 0.40\text{‰}$ ; GR2,  $+2.69 \pm 0.32\text{‰}$ ) specimens. The data from *A. opercularis* and *A. islandica* compare closely with those from early Pliocene examples of these species from eastern England (Johnson et al., 2009; Vignols et al., 2019). The difference between the

means from early Pliocene *A. opercularis* (calcitic) and *A. islandica* (aragonitic) was ascribed principally to the mineralogical difference (Vignols et al., 2019). This interpretation is supported by the mean values from the present *G. radiolyrata* (aragonitic) specimens, which are similar to those from *A. islandica*, but not by the *P. rustica* (also aragonitic) mean value, which is only a little outside the range of mean values from *A. opercularis*. The different pattern of overall ontogenetic change in *G. radiolyrata* and *A. islandica* (increase, unlike in *A. opercularis* and *P. rustica*) also remains to be explained, as does the unusual negative covariation between  $\delta^{13}\text{C}$  and  $\delta^{18}\text{O}$  in *G. radiolyrata*.

## 5.3 Microgrowth-increment patterns (*A. opercularis*)

Even in smoothed (five-point moving average) profiles of microgrowth-increment size from *A. opercularis*, substantial high-frequency variation is present in nearly all cases. However, amongst those profiles long enough to show a low-frequency pattern, in a number of cases a fairly clear and complete major cycle proceeding from small to large to small increments is discernible over about the first 40 mm of shell height. Such a cycle is evident in three of the four Luchtbal Member (and equivalent) profiles, in each case with an amplitude (difference between the maximum and minimum of the smoothed profile) of more than 0.30 mm. The exception (AO4 – Fig. 5a) is a profile too short to show this pattern. Only one (AO6 – Fig. 6g) of the four Oorderen Member (and equivalent) profiles has an amplitude greater than 0.30 mm, but a second (AO5 – Fig. 6f) has an amplitude only fractionally less and a third (AO8 – Fig. 6c) is too short to show equivalent (“high-amplitude”) variation. Despite their considerable length the Merksem-equivalent profiles exhibit an amplitude well below 0.30 mm (“low amplitude”). The prevalent high-amplitude pattern from Luchtbal Member (and equivalent) shells corresponds to that in modern sub-thermocline shells, and the occurrence of the pattern in an Oorderen Member shell is at least inconsistent with a supra-thermocline setting (Johnson et al., 2009, 2021b). The low-amplitude pattern in the two Merksem-equivalent shells is consistent with a supra-thermocline setting; however, given the occasional occurrence of such a pattern in sub-thermocline shells, it is not inconsistent with the latter setting.

## 6 Interpretation

### 6.1 Temperatures

#### 6.1.1 Derivation, comparison, and evaluation of seasonal seafloor values

The equations and water  $\delta^{18}\text{O}$  values that were employed to calculate summer and winter temperatures from shell  $\delta^{18}\text{O}$  are explained in Sect. 4.2. Following the reasoning of Johnson et al. (2017), the shell  $\delta^{18}\text{O}$  values used were the ex-

treme ones at inflection points in profiles, supplemented in the present case by those profile-end values possibly corresponding to inflection points on the evidence of similar (true) inflection-point values from the same and other co-occurring shells of the species concerned. The profile-end values probably provide slight underestimates of summer temperature and slight overestimates of winter temperature in some cases – i.e. had the profiles extended farther, slightly lower or higher  $\delta^{18}\text{O}$  values, respectively, might have been identified. As well as errors from this source, others of the same type no doubt exist in the case of data from locations close to growth breaks (as a result of an incomplete record) and, for at least *A. opercularis*, in the case of late ontogenetic data (as a result of time averaging), although no significant error is likely where the temperatures concerned are higher (for summers) or lower (for winters) than a reliable estimate from another time in ontogeny. Alongside the profile-end and near-growth-break (unreliable) winter  $\delta^{18}\text{O}$  data from *G. radiolyrata* is one inflection-point value (the first, unaccompanied by a growth break, at a height of 17.9 mm in GR2; Fig. 6e) which appears acceptable as a source of reliable temperature information. The  $\delta^{18}\text{O}$  value is, however, lower than any from this taxon regarded as an unreliable source of winter temperatures. Hence, it too must be regarded as suspect, possibly recording a downward temperature fluctuation in spring rather than true winter conditions.

All the calculated temperatures are represented in Fig. 8, those based on equations providing minimum seasonal ranges for *G. radiolyrata* and *A. opercularis* combined in Fig. 8a, those providing maximum seasonal ranges for these species combined in Fig. 8b, and those providing a minimum seasonal range for *G. radiolyrata* and a maximum for *A. opercularis* (a “hybrid” set) combined in Fig. 8c. Unreliable values (probable underestimates for summers and overestimates for winters) are identified by the use of an open symbol, whereby we have applied the above reasoning uniformly except to *G. radiolyrata*, *A. islandica*, and *P. rustica*: in the absence of early ontogenetic data for comparison in these species, we have assumed that the late ontogenetic data represented are free from time-averaging effects.

Figure 8 shows a general similarity in seasonal temperatures within and between stratigraphic members, with the exception of winter values supplied by *G. radiolyrata* from the Luchtbal Member, which are markedly higher than those from Luchtbal Member *A. opercularis*. Since the specimens of each species come from different (although immediately adjacent) beds, it is conceivable that the data reflect environmental change. However, given the fact that the summer temperatures supplied by the species are close or identical (dependent on the method of calculation) and that all of the 12 sets of winter temperatures from *G. radiolyrata* are probable overestimates, it seems much more likely that the change is apparent rather than real. If this is accepted then it is sensible to view those Luchtbal Member (and equivalent) summer temperatures represented in Fig. 8a and c (very similar

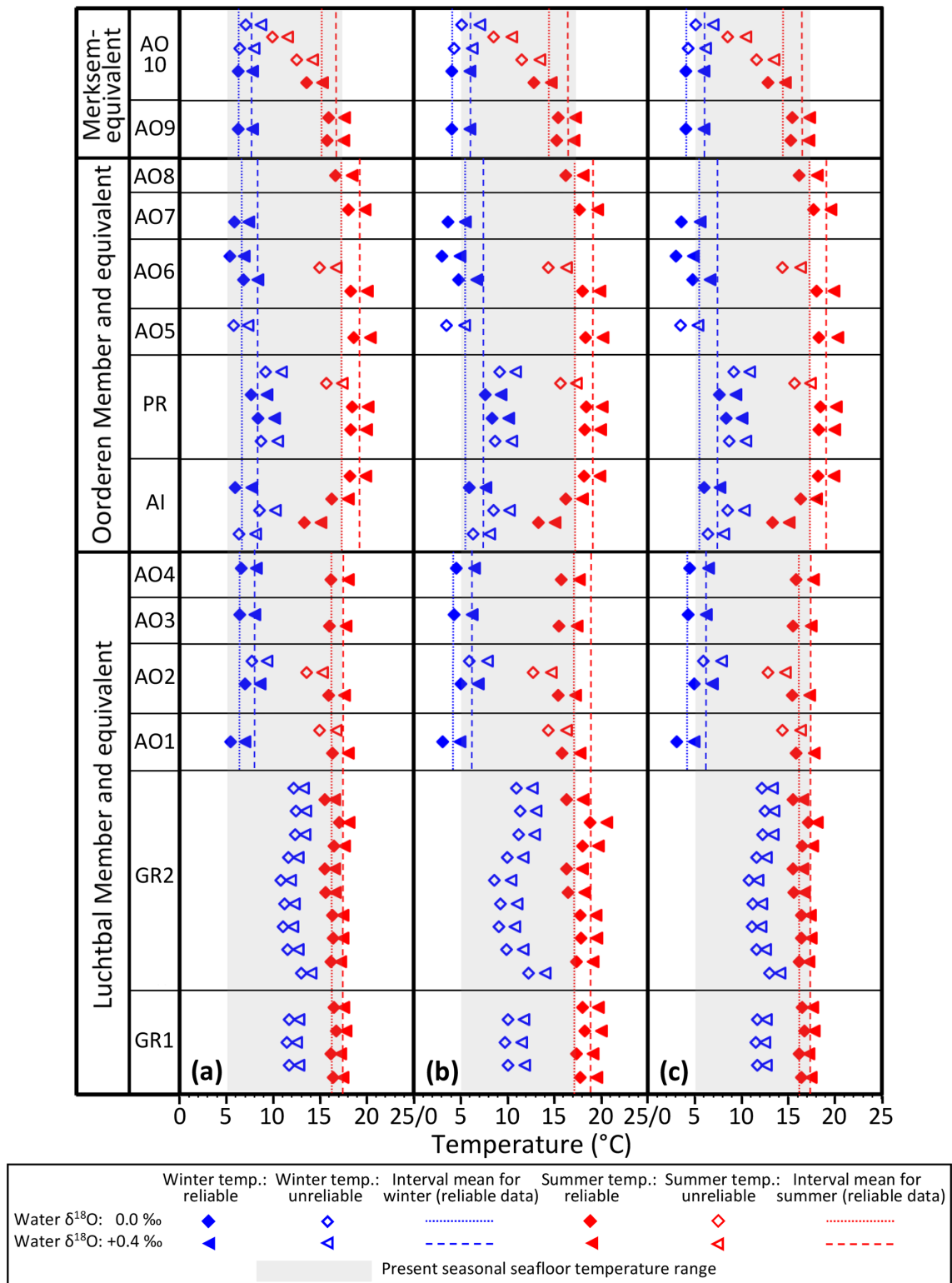
from *G. radiolyrata* and *A. opercularis* for the same water  $\delta^{18}\text{O}$  value) as more accurate than those in Fig. 8b (somewhat lower from *A. opercularis* than from *G. radiolyrata* for the same water  $\delta^{18}\text{O}$  value). The Oorderen Member winter temperatures from *A. islandica* and *P. rustica* are closer to those from Oorderen Member *A. opercularis* (from the same bed) in Fig. 8a than those in Fig. 8c (and Fig. 8b), suggesting that the data in Fig. 8a are the most accurate overall. However, if it is untrue that the winter data from *A. islandica* and *P. rustica* are free from time-averaging effects (i.e. if the data are unreliable), there is no reason for favouring the remaining data in Fig. 8a over those in Fig. 8c.

Table 2 gives the interval mean values for seasonal temperatures based on reliable data, as depicted in Fig. 8. Unlike other changes, the Luchtbal to Oorderen increases and the Oorderen to Merksem decreases in mean summer temperature evident in Fig. 8a and c are statistically significant for both water  $\delta^{18}\text{O}$  values (one-tailed *t* tests;  $p < 0.05$ ). The fact that these changes correspond at least qualitatively to the changes in summer temperature inferred from dinocysts and ostracods (Sect. 3) cements the impression that the data in Fig. 8a and c provide a more accurate picture of seasonal temperatures, and hence of seasonal range, than the data in Fig. 8b, in which only the Oorderen to Merksem decrease in summer temperature (again statistically significant) is evident.

In conclusion, the data in Fig. 8a are probably the most accurate, but the data in Fig. 8c should not be excluded from consideration, especially as evidence from modern *A. opercularis* (Johnson et al., 2021b) suggests that the equation of Bemis et al. (1998), used for the calculation of temperatures from this species in Fig. 8c, provides more accurate temperatures than the equation of O’Neil et al. (1969), used in Fig. 8a.

### 6.1.2 Seasonal seafloor ranges

With the exception of the Luchtbal values resulting from the questionable combination of data employed in Fig. 8b, all the seasonal ranges for members (irrespective of how data have been combined and temperatures calculated; Table 2) are lower than the current seafloor range at offshore locations in the southern North Sea – e.g. at 53° N, 03° E, where the difference between mean maximum and minimum temperatures is 12.2 °C (Johnson et al., 2021b, their Fig. 1a). However, they are only slightly lower (compare the separations of the dotted/dashed lines in Fig. 8 with the width of the grey bar showing the current range at 53° N, 03° E), and not all individual specimens indicate a lower range (Table 3): the *A. islandica* specimen (Oorderen Member) shows the same range as currently at 53° N, 03° E, and even a water  $\delta^{18}\text{O}$  value of 0.0 ‰ used with the equation of O’Neil et al. (1969) yields a range (12.8 °C) from the Oorderen *A. opercularis* specimen AO5 that is higher than at present. The latter case is based on a winter temperature that is not reliable in the sense



**Figure 8.** Winter and summer sea floor temperatures, calculated from the seasonal extreme  $\delta^{18}\text{O}$  values indicated in Figs. 6 and 7, using water  $\delta^{18}\text{O}$  values of 0.0‰ and +0.4‰ and various equations. (a) Equation of Royer et al. (2013) for GR, of O’Neil et al. (1969) for AO and of Grossman and Ku (1986) for AI and PR; (b) equation of Grossman and Ku (1986) for GR, AI, and PR and of Bemis et al. (1998) for AO; (c) equation of Royer et al. (2013) for GR, of Bemis et al. (1998) for AO, and of Grossman and Ku (1986) for AI and PR. Interval means are for reliable seasonal temperatures (see Sect. 6.1.1) from the Luchtbal Member and equivalent, Oorderen Member and equivalent, and Merksem-equivalent strata. The indicated present-day seasonal sea floor temperature range (4.7–16.9 °C) is for 25 m depth at 53° N, 03° E.

**Table 2.** Mean summer (SSFT) and winter (WSFT) seafloor temperatures ( $^{\circ}\text{C}$ ;  $\pm 1\sigma$ ), seasonal range (SFR: SSFT minus WSFT), and annual average temperature (ASFT: midpoint between SSFT and WSFT) for “members”, based on the reliable data indicated in Fig. 8.

| Member and/or equivalent | Water $\delta^{18}\text{O} = 0.0\text{‰}$ |                |               |      | Water $\delta^{18}\text{O} = +0.4\text{‰}$ |                |               |      |      |
|--------------------------|---|----------------|---------------|------|--|----------------|---------------|------|------|
|                          | SSFT                                      | WSFT           | SFR           | ASFT | SSFT                                       | WSFT           | SFR           | ASFT |      |
| Fig. 8a                  | Merksem                                   | $15.1 \pm 1.1$ | $6.2 \pm 0.0$ | 8.9  | 10.7                                       | $16.8 \pm 1.1$ | $7.8 \pm 0.0$ | 9.0  | 12.3 |
|                          | Oorderen                                  | $17.3 \pm 1.6$ | $6.7 \pm 1.0$ | 10.6 | 12.0                                       | $19.1 \pm 1.6$ | $8.3 \pm 1.1$ | 10.8 | 13.7 |
|                          | Luchtbal                                  | $16.2 \pm 0.4$ | $6.4 \pm 0.6$ | 9.8  | 11.3                                       | $17.5 \pm 0.5$ | $8.0 \pm 0.6$ | 9.5  | 12.8 |
| Fig. 8b                  | Merksem                                   | $14.5 \pm 1.2$ | $4.1 \pm 0.0$ | 10.4 | 9.3  | $16.4 \pm 1.2$ | $6.0 \pm 0.0$ | 10.4 | 11.2 |
|                          | Oorderen                                  | $17.2 \pm 1.6$ | $5.6 \pm 2.0$ | 11.6 | 11.4                                       | $19.0 \pm 1.6$ | $7.4 \pm 1.9$ | 11.6 | 13.2 |
|                          | Luchtbal                                  | $17.1 \pm 1.1$ | $4.2 \pm 0.7$ | 12.9 | 10.7                                       | $18.9 \pm 1.0$ | $6.2 \pm 0.7$ | 12.7 | 12.6 |
| Fig. 8c                  | Merksem                                   | $14.5 \pm 1.2$ | $4.1 \pm 0.0$ | 10.4 | 9.3  | $16.4 \pm 1.2$ | $6.0 \pm 0.0$ | 10.4 | 11.2 |
|                          | Oorderen                                  | $17.2 \pm 1.6$ | $5.6 \pm 2.0$ | 11.6 | 11.4                                       | $19.0 \pm 1.6$ | $7.4 \pm 1.9$ | 11.6 | 13.2 |
|                          | Luchtbal                                  | $16.1 \pm 0.5$ | $4.2 \pm 0.7$ | 11.9 | 10.2                                       | $17.4 \pm 0.4$ | $6.2 \pm 0.7$ | 11.2 | 11.8 |

of Sect. 6.1.1, but the true (most extreme) winter temperature can only have been less and the seasonal range hence greater. Using a water  $\delta^{18}\text{O}$  value of  $+0.4\text{‰}$  with the equation of O’Neil et al. (1969) yields a range of  $12.4^{\circ}\text{C}$  from the Oorderen specimen AO7, and using the equation of Bemis et al. (1998) yields a range of  $13.2^{\circ}\text{C}$  from the Oorderen specimen AO6 and  $12.8^{\circ}\text{C}$  from the Luchtbal specimen AO1 (independent of water  $\delta^{18}\text{O}$ ) as well as higher ranges than with the equation of O’Neil et al. (1969) from the Oorderen specimens AO5 ( $14.9^{\circ}\text{C}$ ) and AO7 ( $14.0^{\circ}\text{C}$ ). It can therefore be said that at times during the period of deposition of the Oorderen Member, and possibly of the Luchtbal Member, the seasonal range in seafloor temperature was higher than the current typical range. One should, however, bear in mind the variation of about  $2^{\circ}\text{C}$  either side of the mean maximum and minimum temperatures in the North Sea at present (Lane and Prandle, 1996), so the “high” individual Oorderen and Luchtbal ranges do not necessarily manifest significantly greater seasonality than now. Individual specimens from the equivalent of the Merksem Member provide some evidence of a lower seafloor range than now (maximum range  $11.3^{\circ}\text{C}$  from AO9, calculated with the equation of Bemis et al., 1998), but the small sample size (two) should be noted.

The calculations leading to the above figures for seasonal range assume constant water  $\delta^{18}\text{O}$  during the intervals of ontogeny concerned. If at the times of maximum temperature the actual water  $\delta^{18}\text{O}$  value was lower than assumed the calculated temperatures would be overestimates; similarly, if at the times of minimum temperature the actual water  $\delta^{18}\text{O}$  value was higher than assumed the calculated temperatures would be underestimates. Each of these situations, or the two together, would yield an overestimate of seasonal range. While these circumstances are possible, they are improbable. As noted in Sect. 2, water  $\delta^{18}\text{O}$  is relatively high (not low) during summer and relatively low (not high) during winter

in coastal waters of the North Sea at present. The calculated seasonal ranges are thus more likely to be underestimates.

### 6.1.3 Seasonal surface ranges

The water depths indicated by the bivalve mollusc assemblages of the Luchtbal and Oorderen members (respective minimum depths 40 and 35 m; Sect. 3) are greater than the typical depth of the summer thermocline in shelf settings (25–30 m). Microgrowth-increment evidence from *A. opercularis* (Sect. 5.3) is consistent with a sub-thermocline setting for both members, and the higher frequency of such evidence from the Luchtbal Member is consistent with the indication from assemblage analysis that this was deposited at a greater depth than the Oorderen Member. Microgrowth-increment evidence of a supra-thermocline setting from Merksem-equivalent shells in the Oosterhout Formation at Ouwerkerk is similarly consistent with the shallow depth of deposition (maximum 15 m) indicated by the biota of the Merksem Member itself at Antwerp (note that supra-thermocline settings exist now in the southern North Sea at a distance from the shore well beyond that of Ouwerkerk from the Pliocene shoreline; Fig. 2). Given a sub-thermocline setting for the Luchtbal and Oorderen members we must add a “stratification factor” to summer seafloor temperatures to derive estimates of summer surface temperature and hence seasonal surface range (winter surface temperature is likely to have been the same as on the seafloor; Johnson et al., 2021b). There is a difference of  $2.6^{\circ}\text{C}$  between the mean annual seafloor and surface temperature maxima at a seasonally stratified location (depth 59 m) in the central North Sea some 600 km north of the sites of the Pliocene shells (Johnson et al., 2021b). At this location the mean maximum surface temperature is only  $13.7^{\circ}\text{C}$ , a figure substantially exceeded in the (unstratified) southern North Sea at present (e.g.  $17.1^{\circ}\text{C}$  at  $53^{\circ}\text{N}$ ,  $03^{\circ}\text{E}$ ; Johnson et al., 2021b, their Fig. 1a) and with little doubt at warm times during the deposition of

**Table 3.** Summer (SSFT) and winter (WSFT) seafloor temperatures (°C) for the year showing the greatest range (SFR; SSFT minus WSFT) from each shell, together with the annual average seafloor temperature (ASFT; midpoint between SSFT and WSFT). Unreliable as well as reliable seasonal temperatures used (Fig. 8). AO8 (no winter data) has been included to supplement the summer data.

| Member and/or equivalent | Shell | Temperatures using the equations of O'Neil et al. (1969) for AO, Royer et al. (2013) for GR, Grossman and Ku (1986) for AI and PR |      |      |                                 |      |      | Temperatures using the equations of Bemis et al. (1998) for AO, Grossman and Ku (1986) for GR |      |      |                                 |      |      |      |      |      |      |
|--------------------------|-------|---|------|------|---------------------------------|------|------|---|------|------|---------------------------------|------|------|------|------|------|------|
|                          |       | Water δ <sup>18</sup> O = 0.0‰  |      |      | Water δ <sup>18</sup> O = +0.4‰ |      |      | Water δ <sup>18</sup> O = 0.0‰  |      |      | Water δ <sup>18</sup> O = +0.4‰ |      |      |      |      |      |      |
|                          |       | SSFT  | WSFT | SFR  | ASFT                            | SSFT | WSFT | SFR   | ASFT | SSFT | WSFT                            | SFR  | ASFT | SSFT | WSFT | SFR  | ASFT |
| Merksem                  | AO10  | 13.6  | 6.2  | 7.4  | 9.9                             | 15.3 | 7.8  | 7.5   | 11.6 | 12.8 | 4.1                             | 8.7  | 8.5  | 14.7 | 6.0  | 8.7  | 10.4 |
|                          | AO9   | 15.9  | 6.2  | 9.7  | 11.1                            | 17.6 | 7.8  | 9.8   | 12.7 | 15.4 | 4.1                             | 11.3 | 9.8  | 17.3 | 6.0  | 11.3 | 11.7 |
| Oorderen                 | AO8   | 16.6  |      |      |                                 | 18.4 |      |   |      | 16.2 |                                 |      |      | 18.1 |      |      |      |
|                          | AO7   | 18.0  | 5.9  | 12.1 | 12.0                            | 19.8 | 7.4  | 12.4  | 13.6 | 17.7 | 3.6                             | 14.1 | 10.7 | 19.6 | 5.6  | 14.0 | 12.6 |
|                          | AO6   | 18.3  | 6.8  | 11.5 | 12.6                            | 20.1 | 8.4  | 11.7  | 14.3 | 18.0 | 4.8                             | 13.2 | 11.4 | 19.9 | 6.7  | 13.2 | 13.3 |
|                          | AO5   | 18.6  | 5.8  | 12.8 | 12.2                            | 20.4 | 7.3  | 13.1  | 13.9 | 18.3 | 3.5                             | 14.8 | 10.9 | 20.3 | 5.4  | 14.9 | 12.9 |
|                          | PR    | 18.4  | 7.6  | 10.8 | 13.0                            | 20.1 | 9.4  | 10.7  | 14.8 |      |                                 |      |      |      |      |      |      |
| AI                       | 18.2  | 6.0   | 12.2 | 12.1 | 19.9                            | 7.7  | 12.2 | 13.8  |      |      |                                 |      |      |      |      |      |      |
| Luchtbal                 | AO4   | 16.2  | 6.6  | 9.6  | 11.4                            | 18.0 | 8.2  | 9.8   | 13.1 | 15.8 | 4.5                             | 11.3 | 10.2 | 17.7 | 6.5  | 11.2 | 12.1 |
|                          | AO3   | 16.0  | 6.4  | 9.6  | 11.2                            | 17.8 | 8.0  | 9.8   | 12.9 | 15.5 | 4.3                             | 11.2 | 9.9  | 17.5 | 6.3  | 11.2 | 11.9 |
|                          | AO2   | 15.9  | 7.0  | 8.9  | 11.5                            | 17.6 | 8.6  | 9.0   | 13.1 | 15.4 | 5.0                             | 10.4 | 10.2 | 17.3 | 6.9  | 10.4 | 12.1 |
|                          | AO1   | 16.3  | 5.4  | 10.9 | 10.9                            | 18.0 | 7.0  | 11.0  | 12.5 | 15.8 | 3.1                             | 12.7 | 9.5  | 17.8 | 5.0  | 12.8 | 11.4 |
|                          | GR2   | 16.4  | 11.1 | 5.3  | 13.8                            | 17.5 | 12.1 | 5.4   | 14.8 | 17.9 | 9.1                             | 8.8  | 13.5 | 19.6 | 10.8 | 8.8  | 15.2 |
|                          | GR1   | 16.7  | 11.5 | 5.2  | 14.1                            | 17.8 | 12.5 | 5.3   | 15.2 | 18.3 | 9.8                             | 8.5  | 14.1 | 20.0 | 11.5 | 8.5  | 15.8 |

the Oorderen Member (see Sect. 3). From the evidence of dinocysts (De Schepper et al., 2009) it is conceivable that at cool times, and during the deposition of the Luchtbal Member, summer surface temperature was not much higher than the present central North Sea figure. A stratification factor of 3 °C is therefore a reasonable estimate for these cool intervals and a serviceable (conservative) one for warm intervals during the deposition of the Oorderen Member. Adding 3 °C to the interval mean values for Luchtbal and Oorderen summer seafloor temperature yields stratification-adjusted figures for seasonal surface range (Table 4) that are in all cases higher than the present typical range in the southern North Sea (12.4 °C at 53° N, 03° E; Johnson et al., 2021b). Adding the same to individual values also yields figures for seasonal surface range (Table 5) that are higher than the present typical range, except in the cases of Luchtbal specimens GR1, GR2, and AO2. A lower range is only obtained from the last when benthic temperature is calculated using the equation of O'Neil et al. (1969), and the lower ranges from GR1 and GR2 reflect the high winter seafloor temperatures recorded, all of which are unreliable. While the Luchtbal and Oorderen (and respective equivalent) shells provide clear evidence of a higher surface range than now (see Fig. 9, which depicts the interval mean and individual information from Tables 4 and 5), a lower range is indicated by the two Merksem-equivalent shells, assuming these have been correctly interpreted as from a supra-thermocline setting. It may of course be the case that they provide an unrepresentative picture for their time.

### 6.1.4 Absolute surface temperatures

As pointed out in Sect. 6.1.1, there is a Luchtbal–Oorderen increase and an Oorderen–Merksem decrease in mean summer seafloor temperature from reliable individual summer values calculated using the equation of Royer et al. (2013) for *G. radiolyrata*, the equation of Grossman and Ku (1986) for *A. islandica* and *P. rustica*, and the equations of both O'Neil et al. (1969) and Bemis et al. (1998) for *A. opercularis*. These changes are evident whether a water δ<sup>18</sup>O value of 0.0‰ or +0.4‰ is applied, are statistically significant, and correspond qualitatively to changes in summer temperature inferred from assemblages of ostracods and dinocysts. These proxies (and organic biomarkers – see below) provide estimates that are time-averaged to much the same extent as the interval-mean seasonal temperatures quoted herein, making comparison fair. The data from ostracods and probably from dinocysts relate to summer sea surface temperature (SSST), so quantitative comparison must involve the equivalent data, derived as indicated in Sect. 6.1.3. The relevant interval mean information is that for Fig. 9a and c in Table 4, showing Oorderen SSST above 20 °C and Merksem SSST below 20 °C, irrespective of the water δ<sup>18</sup>O value used in calculation, and Luchtbal SSST above 20 °C with a water δ<sup>18</sup>O value of +0.4‰ and below 20 °C with a water δ<sup>18</sup>O value of

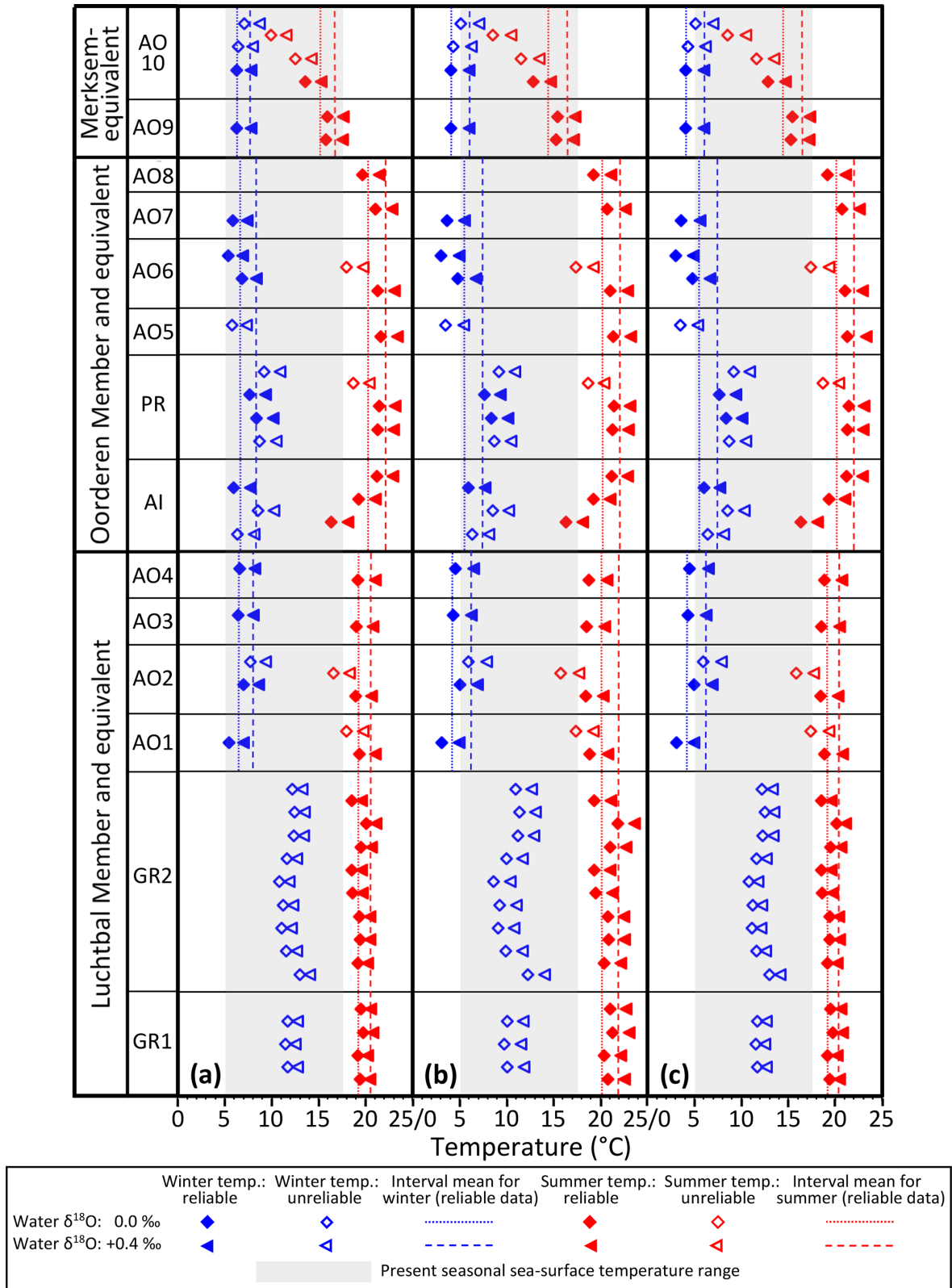


**Figure 9.** Winter and summer sea surface temperatures, calculated as in Fig. 8, using the same equations for (a), (b), and (c) but with a 3 °C supplement to Luchtbal and Oorderen summer temperatures in recognition of thermal stratification (see text, Sect. 6.1.3, for explanation). Interval means calculated as in Fig. 8. The indicated present-day seasonal sea surface temperature range (4.7–17.1 °C) is for 53° N, 03° E. Note that the Luchtbal and Oorderen ranges, as indicated by the separation of dotted or dashed lines for each interval, are larger than the present-day range (see text, Sect. 6.1.3, for more detailed discussion).

**Table 4.** Mean summer (SSST) and winter (WSST) sea surface temperatures ( $^{\circ}\text{C}$ ;  $\pm 1\sigma$ ), seasonal range (SSR: SSST minus WSST), and annual average temperature (ASST: midpoint between SSST and WSST) for “members”, based on the reliable data indicated in Fig. 8, with a  $3^{\circ}\text{C}$  addition to Luchtbal and Oorderen summer seafloor temperatures in recognition of summer stratification (see text, Sect. 6.1.3, for explanation).

| Member and/or equivalent |          | Water $\delta^{18}\text{O} = 0.0\text{‰}$ |               |      |      | Water $\delta^{18}\text{O} = +0.4\text{‰}$ |               |      |      |
|--------------------------|----------|---|---------------|------|------|--|---------------|------|------|
|                          |          | SSST                                      | WSST          | SSR  | ASST | SSST                                       | WSST          | SSR  | ASST |
| Fig. 9a                  | Merksem  | $15.1 \pm 1.1$                            | $6.2 \pm 0.0$ | 8.9  | 10.7 | $16.8 \pm 1.1$                             | $7.8 \pm 0.0$ | 9.0  | 12.3 |
|                          | Oorderen | $20.3 \pm 1.6$                            | $6.7 \pm 1.0$ | 13.6 | 13.5 | $22.1 \pm 1.6$                             | $8.3 \pm 1.1$ | 13.8 | 15.2 |
|                          | Luchtbal | $19.2 \pm 0.4$                            | $6.4 \pm 0.6$ | 12.8 | 12.8 | $20.5 \pm 0.5$                             | $8.0 \pm 0.6$ | 12.5 | 14.3 |
| Fig. 9b                  | Merksem  | $14.5 \pm 1.2$                            | $4.1 \pm 0.0$ | 10.4 | 9.3  | $16.4 \pm 1.2$                             | $6.0 \pm 0.0$ | 10.4 | 11.2 |
|                          | Oorderen | $20.2 \pm 1.6$                            | $5.6 \pm 2.0$ | 14.6 | 12.9 | $22.0 \pm 1.6$                             | $7.4 \pm 1.9$ | 14.6 | 14.7 |
|                          | Luchtbal | $20.1 \pm 1.1$                            | $4.2 \pm 0.7$ | 15.9 | 12.2 | $21.9 \pm 1.0$                             | $6.2 \pm 0.7$ | 15.7 | 14.1 |
| Fig. 9c                  | Merksem  | $14.5 \pm 1.2$                            | $4.1 \pm 0.0$ | 10.4 | 9.3  | $16.4 \pm 1.2$                             | $6.0 \pm 0.0$ | 10.4 | 11.2 |
|                          | Oorderen | $20.2 \pm 1.6$                            | $5.6 \pm 2.0$ | 14.6 | 12.9 | $22.0 \pm 1.6$                             | $7.4 \pm 1.9$ | 14.6 | 14.7 |
|                          | Luchtbal | $19.1 \pm 0.5$                            | $4.2 \pm 0.7$ | 14.9 | 11.7 | $20.4 \pm 0.4$                             | $6.2 \pm 0.7$ | 14.2 | 13.3 |

$0.0\text{‰}$ . All the Oorderen SSST estimates are consistent with dinocyst evidence (Sect. 3) specifying mainly warm temperate conditions (SSST  $> 20^{\circ}\text{C}$ ; Johnson et al., 2021b), and the Luchtbal SSST estimates with a water value of  $0.0\text{‰}$  are consistent with dinocyst evidence specifying cool temperate conditions (SSST  $< 20^{\circ}\text{C}$ ; Johnson et al., 2021b). This suggests that temperatures calculated with a water  $\delta^{18}\text{O}$  value of  $0.0\text{‰}$  may be the most accurate for all intervals. The Merksem interval mean SSST calculated with this value is  $14.5$  or  $15.1^{\circ}\text{C}$  dependent on the equation used (Table 4), both figures being consistent with the Oorderen–Merksem SSST decrease of  $5\text{--}6^{\circ}\text{C}$  indicated by ostracod assemblage data (Sect. 3). The statements made in respect of interval means also apply in general to individual SSST values calculated with the same equations (Table 5). The only exceptions are the temperatures derived using a water  $\delta^{18}\text{O}$  value of  $0.0\text{‰}$  from Oorderen specimen AO8, which are slightly below the warm temperate range for summer. Such temperatures are entirely to be expected from some individuals in a regime with a mean SSST only a few degrees above the cool temperate range (see Sect. 6.1.2).

The similarity of  $\delta^{18}\text{O}$ -derived estimates of summer sea surface temperature, particularly those using a water  $\delta^{18}\text{O}$  value of  $0.0\text{‰}$ , to assemblage-based estimates lends credence to the equivalent winter sea surface temperatures (WSSTs). With the exception only of unreliable individual data from *G. radiolyrata*, all WSST estimates (Tables 4, 5) are firmly in the cool temperate range ( $< 10^{\circ}\text{C}$ ; Johnson et al., 2021b). We can take the midpoint between interval mean SSST and WSST estimates as a figure for annual (“average”) sea surface temperature (ASST) and compare this with ASST estimates based on other information. Robinson et al. (2018) derived an ASST of  $13.6^{\circ}\text{C}$  for the mid-Piacenzian North Sea using bivalve  $\delta^{18}\text{O}$  data from the Coralline Crag Forma-

tion (UK). It is, however, questionable whether the Coralline Crag is of this age (see Fig. 3). Dearing Crampton-Flood et al. (2020) obtained an SSST of about  $16^{\circ}\text{C}$  (cool temperate) from alkenone index and a WSST of about  $10^{\circ}\text{C}$  (boundary cool–warm temperate) from  $\text{TEX}_{86}$  for part of the Oosterhout Formation in the Netherlands (Noord-Brabant) representing the MPWP. These figures specify an ASST of  $13^{\circ}\text{C}$ . This is very similar to the  $\delta^{18}\text{O}$ -derived ASST estimates (Table 4) of  $12.9$  and  $13.5^{\circ}\text{C}$  obtained using a water  $\delta^{18}\text{O}$  value of  $0.0\text{‰}$  from Oorderen and equivalent shells, which represent the same interval. Such figures for ASST ( $2\text{--}3^{\circ}\text{C}$  higher than the modern ASST of  $10.9^{\circ}\text{C}$  specified by an SSST of  $17.1^{\circ}\text{C}$  and WSST of  $4.7^{\circ}\text{C}$  at  $53^{\circ}\text{N}$ ,  $03^{\circ}\text{E}$ ; Johnson et al., 2021b, their Fig. 1a) are entirely consistent with general expectations for the MPWP, but the  $\delta^{18}\text{O}$ -derived data reveal that they result from substantially warmer summer conditions than at present and winter conditions much the same as now, opposite to the picture provided by alkenone and  $\text{TEX}_{86}$  data. The interval mean Luchtbal figures for SSST obtained using a water  $\delta^{18}\text{O}$  value of  $0.0\text{‰}$  are likewise above the present SSST, although less markedly so, and in combination with WSST figures similar to the present also specify a higher ASST than now (Table 4). By contrast, the equivalent Merksem figures for SSST are below the present value and in combination with WSST figures similar to the present specify a lower ASST than now.

## 6.2 Meaning of $\delta^{13}\text{C}$ data

The ontogenetic decline in  $\delta^{13}\text{C}$  shown by *A. opercularis* is as seen in modern examples of the species from diverse settings (Johnson et al., 2021b) and probably reflects increasing output of isotopically light respiratory carbon with increasing body size alongside slower shell secretion – i.e. reduced “demand” for carbon (Lorrain et al., 2004). Short-term fluctua-

tions paralleling changes in  $\delta^{18}\text{O}$  might similarly reflect variation in respiratory output determined by seasonal variation in the availability of food (Chauvaud et al., 2011). The opposite ontogenetic trend shown by *G. radiolyrata* and *A. islandica* can hardly be explained by a reduction in respiratory output, and the opposite short-term pattern shown by *G. radiolyrata* is unlikely to reflect a reversal in the timing of maximum food availability from summer to winter. These changes might reflect variation in the  $\delta^{13}\text{C}$  of dissolved inorganic carbon (DIC), the main source of carbon in shells (Marchais et al., 2015). Preferential uptake of  $^{12}\text{C}$  by photosynthesizers is a major influence on the  $\delta^{13}\text{C}$  of DIC, but high photosynthetic fixation of carbon in summer is a doubtful cause of the high summer  $\delta^{13}\text{C}$  values in *G. radiolyrata* because it would require (see Arthur et al., 1983) that the shells lived above the thermocline, which other evidence argues against. The anomalously low  $\delta^{13}\text{C}$  values from *P. rustica* (for the aragonite mineralogy) cannot be explained as a consequence of the incorporation of isotopically light carbon from porewaters (cf. Krantz et al., 1987) because the other infaunal species, *G. radiolyrata* and *A. islandica*, exhibit high values. Conceivably, the *P. rustica* values reflect a food source with a particularly low value (Marchais et al., 2015).

In view of the multiple potential “local” controls on shell  $\delta^{13}\text{C}$  it is questionable whether the relatively low values from late Pliocene *A. opercularis*, compared to pre-industrial Holocene examples (Hickson et al., 2000), are a reflection of relatively high atmospheric  $\text{CO}_2$ , as was previously suggested to explain the similarly low values from early Pliocene forms (Johnson et al., 2009; Vignols et al., 2019).

## 7 Implications of temperature data

We have shown that by adopting certain equations relating shell  $\delta^{18}\text{O}$  to temperature, selecting a particular modelled value for water  $\delta^{18}\text{O}$ , and making a reasonable allowance for summer stratification (where indicated by independent evidence), it is possible to generate summer surface temperatures from shell  $\delta^{18}\text{O}$  data that are consistent with assemblage-derived estimates (cool or warm temperate according to interval) for the late Pliocene of Belgium and the Netherlands. The corresponding winter surface temperatures are cool temperate in each of the three (Luchtbal, Oorderen, and Merksem) intervals studied and in conjunction with the summer temperatures demonstrate a higher seasonal surface range than at present in the area during the Luchtbal and Oorderen intervals. Age and independent environmental information (Sect. 3) preclude interpretation of the Luchtbal and Oorderen data as a reflection of glacial episodes, when seasonality appears to be enhanced (Hennissen et al., 2015; Crippa et al., 2016) – i.e. the different seasonality from now was under equivalent overall conditions (interglacial).

The approach used herein has also revealed high seasonal surface ranges in the early Pliocene of the SNSB and the

early and late Pliocene of the eastern seaboard of the USA (Johnson et al., 2017, 2019, 2021b; Vignols et al. 2019). Southward-flowing cool currents, as exist now (north of Cape Hatteras), were probably influential in the latter area, but no such current exists at present in the North Sea or is likely to have done during the Pliocene. Presently, winter temperature is raised somewhat in the North Sea by offshoots of the warm North Atlantic Current, principally entering from the north (Winther and Johannessen, 2006). Reduction in this oceanic heat supply, in conjunction with global (atmospheric) warmth, might perhaps have led to the seasonal surface temperatures of the Luchtbal and Oorderen intervals (similar to now in winter, warmer than now in summer) that account for the enhanced seasonal ranges. Raffi et al. (1985) made essentially the same suggestion to explain evidence of high Pliocene seasonality in the southern North Sea from the bivalve assemblage. Fluctuations in the strength and position of the North Atlantic Current during the Pliocene are certainly recognized from proxy evidence, and episodes of reduced oceanic heat supply could correspond to the Luchtbal and Oorderen intervals (e.g. Bachem et al., 2017; Panitz et al., 2018). For the latter (i.e. the MPWP) most models indicate an increase in ocean heat transport in the North Atlantic compared to now, but some indicate a decrease (Zhang et al., 2021). However, even if the times of high seasonality in the SNSB correspond to periods of reduced oceanic heat supply (relative to the Pliocene norm or to the present) it is not yet clear that this is a sufficient explanation for the low winter temperatures contributing to pronounced seasonality. The Merksem decline in summer temperature (post-dating the MPWP) can be more certainly attributed to the global cooling which presaged the onset of Northern Hemisphere glaciation. The lack of a decline in winter temperature is consistent with Mg/Ca evidence from North Atlantic *Globigerina bulloides* (Foraminifera) suggesting that minimum temperatures did not start falling until the very end of the Pliocene, after the time of the deposition of the Lillo Formation (Hennissen et al., 2015, 2017).

The similarity of the alkenone/TEX<sub>86</sub>-based estimate of ASST for the MPWP in the eastern SNSB to the sclerochronologically derived estimates both corroborates the latter and suggests that alkenone temperatures for other areas could be usefully supplemented by information from TEX<sub>86</sub>, even if this would be unlikely to specify the full seasonal range. Combined (average) figures would probably be lower than alkenone-only estimates, and the relatively close alignment of proxy with model temperatures recently achieved for the northern North Atlantic (Sect. 1) might be lost, with implications for model adequacy. Alkenone temperatures for the MPWP in the US Middle Atlantic Coastal Plain are, like those for this interval in the eastern SNSB, similar to summer surface figures based on sclerochronology (Dowsett et al., 2021) and very much higher than winter temperatures derived by this means (Johnson et al., 2017, 2019). The need for “moderation” by winter proxy data in order to facili-

tate meaningful proxy–model comparison is therefore underlined.

The summer seafloor temperatures recorded from a late Pliocene *A. islandica* specimen herein (18.2 and 19.9 °C using water  $\delta^{18}\text{O}$  values of 0.0 and +0.4 ‰, respectively) corroborate evidence supplied by an early Pleistocene example from Italy (20.3 °C from specimen ACG254-1 using a water  $\delta^{18}\text{O}$  value of +0.5 ‰; Crippa et al., 2016, their Table 1) of a thermal range greater in the past than at present (upper limit 16 °C; Witbaard and Bergman, 2003). This indication of change in realized thermal niche supplements evidence of the same in several other bivalve taxa from the early Pliocene of the UK, although in most of these cases it is manifested by tolerance then of winter conditions cooler than are experienced by modern representatives or relatives, which are restricted to Mediterranean locations (Vignols et al., 2019). This information raises some doubts about the use of assemblage evidence to interpret past environments by means of ecological uniformitarianism, the very widely applied approach which assumes that ancient examples of taxa occupied the same niche as modern ones. Certainly the accuracy of this methodology for times beyond the recent past deserves reconsideration.

### 8 Further work

Even if the analysed shells of Luchtbal and Oorderen age were to be from supra- rather than sub-thermocline settings, the  $\delta^{18}\text{O}$  data from them would specify a seasonal surface temperature range much higher than previously inferred – for example, the majority of shells of Oorderen age indicate a range more than double the 6 °C suggested by organic proxies (see Sect. 6.1.4 and the SFR data in Table 3). We argued in Sect. 2 and Sect. 6.1.2 that seasonal variation in shell  $\delta^{18}\text{O}$  is unlikely to have been enhanced by variation in water  $\delta^{18}\text{O}$ , and it can be added here that fluvial input (the means by which variation in water  $\delta^{18}\text{O}$  might have been brought about) may have been less in the Pliocene than now due to a smaller catchment area of the Rhine–Meuse–Scheldt system (Dearing Crampton–Flood et al., 2020), making enhancement of shell  $\delta^{18}\text{O}$  variation by water  $\delta^{18}\text{O}$  variation even more improbable. Notwithstanding these arguments, actual evidence of water  $\delta^{18}\text{O}$  would be very welcome, both as a check on the stability of values through the year and as a means of deriving accurate absolute temperatures. At present, substitution of independently derived temperatures (e.g. from carbonate clumped isotope or biomineral unit thermometry; Briard et al., 2020; Höche et al., 2020, 2021; Caldarescu et al., 2021; de Winter et al., 2021) into equations relating shell  $\delta^{18}\text{O}$  to temperature and water  $\delta^{18}\text{O}$  seems the best approach to determining the last parameter. However, the existence of fluid inclusions in bivalve shell carbonate (Nooitgedacht et al., 2021) raises the possibility that these might serve as a

**Table 5.** Summer (SSST) and winter (WSST) sea surface temperatures (°C) for the year showing the greatest range (SSR; SSST minus WSST) from each shell, together with the annual average sea surface temperature (ASST; midpoint between SSST and WSST). SSST: same as SSFT for Merkssem-equivalent shells; SSFT +3 °C for Luchtbal and Oorderen (and equivalent) shells (see text, Sect. 6.1.3, for explanation). Unreliable as well as reliable seasonal temperatures used (Fig. 9). AO8 (no winter data) has been included to supplement the summer data.

| Member and/or equivalent | Shell | Temperatures using the equations of O’Neil et al. (1969) for AO, Royer et al. (2013) for GR, Grossman and Ku (1986) for AI and PR |      |      |      |      |  |      |      |      |      | Temperatures using the equations of Bemis et al. (1998) for AO, Grossman and Ku (1986) for GR |      |      |      |      |  |      |     |      |      |
|--------------------------|-------|---|------|------|------|------|--|------|------|------|------|---|------|------|------|------|--|------|-----|------|------|
|                          |       | Water $\delta^{18}\text{O} = 0.0\text{‰}$   |      |      |      |      | Water $\delta^{18}\text{O} = +0.4\text{‰}$ |      |      |      |      | Water $\delta^{18}\text{O} = 0.0\text{‰}$   |      |      |      |      | Water $\delta^{18}\text{O} = +0.4\text{‰}$ |      |     |      |      |
|                          |       | SSST  | WSST | SSR  | ASST | ASST | SSST                                       | WSST | SSR  | ASST | ASST | SSST  | WSST | SSR  | ASST | ASST | SSST                                       | WSST | SSR | ASST | ASST |
| Merkssem                 | AO10  | 13.6  | 6.2  | 7.4  | 9.9  | 15.3 | 7.8  | 7.5  | 11.6 | 12.8 | 4.1  | 8.7   | 8.5  | 14.7 | 6.0  | 8.7  | 10.4                                       |      |     |      |      |
|                          | AO9   | 15.9  | 6.2  | 9.7  | 11.1 | 17.6 | 7.8  | 9.8  | 12.7 | 15.4 | 4.1  | 11.3  | 9.8  | 17.3 | 6.0  | 11.3 | 11.7                                       |      |     |      |      |
| Oorderen                 | AO8   | 19.6  |      |      |      | 21.4 |  |      |      | 19.2 |      |   |      | 21.1 |      |      |  |      |     |      |      |
|                          | AO7   | 21.0  | 5.9  | 15.1 | 13.5 | 22.8 | 7.4  | 15.4 | 15.1 | 20.7 | 3.6  | 17.1  | 12.2 | 22.6 | 5.6  | 17.0 | 14.1                                       |      |     |      |      |
|                          | AO6   | 21.3  | 6.8  | 14.5 | 14.1 | 23.1 | 8.4  | 14.7 | 15.8 | 21.0 | 4.8  | 16.2  | 12.9 | 22.9 | 6.7  | 16.2 | 14.8                                       |      |     |      |      |
|                          | AO5   | 21.6  | 5.8  | 15.8 | 13.7 | 23.4 | 7.3  | 16.1 | 15.4 | 21.3 | 3.5  | 17.8  | 12.4 | 23.3 | 5.4  | 17.9 | 14.4                                       |      |     |      |      |
|                          | PR    | 21.4  | 7.6  | 13.8 | 14.5 | 23.1 | 9.4  | 13.7 | 16.3 |      |      |   |      |      |      |      |  |      |     |      |      |
|                          | AI    | 21.2  | 6.0  | 15.2 | 13.6 | 22.9 | 7.7  | 15.2 | 15.3 |      |      |   |      |      |      |      |  |      |     |      |      |
| Luchtbal                 | AO4   | 19.2  | 6.6  | 12.6 | 12.9 | 21.0 | 8.2  | 12.8 | 14.6 | 18.8 | 4.5  | 14.3  | 11.7 | 20.7 | 6.5  | 14.2 | 13.6                                       |      |     |      |      |
|                          | AO3   | 19.0  | 6.4  | 12.6 | 12.7 | 20.8 | 8.0  | 12.8 | 14.4 | 18.5 | 4.3  | 14.2  | 11.4 | 20.5 | 6.3  | 14.2 | 13.4                                       |      |     |      |      |
|                          | AO2   | 18.9  | 7.0  | 11.9 | 13.0 | 20.6 | 8.6  | 12.0 | 14.6 | 18.4 | 5.0  | 13.4  | 11.7 | 20.3 | 6.9  | 13.4 | 13.6                                       |      |     |      |      |
|                          | AO1   | 19.3  | 5.4  | 13.9 | 12.4 | 21.0 | 7.0  | 14.0 | 14.0 | 18.8 | 3.1  | 15.7  | 11.0 | 20.8 | 5.0  | 15.8 | 12.9                                       |      |     |      |      |
|                          | GR2   | 19.4  | 11.1 | 8.3  | 15.3 | 20.5 | 12.1                                       | 8.4  | 16.3 | 20.9 | 9.1  | 11.8  | 15.0 | 22.6 | 10.8 | 11.8 | 16.7                                       |      |     |      |      |
|                          | GRI   | 19.7  | 11.5 | 8.2  | 15.6 | 20.8 | 12.5                                       | 8.3  | 16.7 | 21.3 | 9.8  | 11.5  | 15.6 | 23.0 | 11.5 | 11.5 | 17.3                                       |      |     |      |      |

source of direct insight into the isotopic composition of ambient water during life.

It would, of course, also be useful to have additional shell  $\delta^{18}\text{O}$  (and increment) data, more to confirm the declines in SSST, ASST, and SSR indicated by the limited information from Merksem-age shells than to expand the already substantial evidence of high values for these parameters from shells of Luchtbal and Oorderen age. Notwithstanding some doubts about the reliability of the approach (Johnson et al., 2017), it would also be worth obtaining independent evidence of seasonality from variation in the size of zooids within bryozoan colonies. Using this technique, Knowles et al. (2009, their Table 3) obtained locality-specific seasonality estimates of  $8.08 \pm 1.38$  and  $8.15 \pm 1.30$  °C for the early Pliocene Ramsholt Member of eastern England, figures comparing closely with the estimate of  $7.77 \pm 1.12$  °C obtained through isotope sclerochronology of *A. opercularis* from this unit (mean difference between the winter and summer seafloor temperatures in Johnson et al., 2021b, their Table 3).

In addition to the above refinements of proxy evidence, further modelling efforts are required to see whether the low winter temperatures indicated by sclerochronological evidence for the mid-Piacenzian SNSB can be reproduced and whether reduced oceanic heat supply is a feasible cause. Haywood et al. (2000) modelled mid-Piacenzian summer surface temperatures 2–4 °C higher than at present for the area, similar to those determined herein. However, they modelled winter temperatures 4–6 °C higher than at present, approaching or into the warm temperate range and markedly above the firmly cool temperate values indicated by sclerochronology. Haywood et al. (2000) ascribed the reduced seasonality specified by their results to greater westerly wind stress and strength in the North Atlantic compared to now, with a resultant increase in heat transport by the Gulf Stream and North Atlantic Current. More recent modelling of mid-Piacenzian seasonal sea surface temperatures at higher northern latitudes indicates greater warming in summer than winter (de Nooijer et al., 2020) – i.e. higher seasonality than now, as inferred for the SNSB. Moreover, as already noted (Sect. 7), oceanic heat supply may not have been greater in the mid-Piacenzian. Possibly, the use of up-to-date models with revised boundary conditions may yield results conforming with the evidence of low winter temperatures and high seasonality from the SNSB.

## 9 Conclusions

Sclerochronological evidence from bivalves indicates that for most of the late Pliocene (including the MPWP) the seasonal range in surface temperature in the SNSB was higher than now. This was probably a consequence of higher summer temperatures associated with global (atmospheric) warmth. The apparently similar winter temperatures to now may reflect partial withdrawal of oceanic heat supply to the region

through a change in strength and/or position of the North Atlantic Current.

Averaging sclerochronologically derived summer and winter temperatures yields an annual sea surface temperature 2–3 °C higher than now in the SNSB, as does averaging temperatures from alkenone and TEX<sub>86</sub> thermometry. However, alkenones provide underestimates of extreme summer temperature and TEX<sub>86</sub> provides overestimates of extreme winter temperature; hence these proxies do not specify the full seasonal range. The sclerochronologically derived temperatures are based on shell  $\delta^{18}\text{O}$  and dependent on estimates of water  $\delta^{18}\text{O}$  that require testing. Back-calculation from temperatures obtained by carbonate clumped isotope or biomineral unit thermometry from the same shells constitutes a potential means.

**Data availability.** The raw isotope and increment data, and the corresponding shell heights, are available in the open-source online repository Zenodo (<https://doi.org/10.5281/zenodo.5585630>; Johnson et al., 2021c).

**Author contributions.** ALAJ conceived the study, obtained financial support and access to isotope analytical facilities, conducted some of the isotopic sampling and treatment of results, and drafted the paper. AMV conducted the rest of the isotopic sampling and treatment of results and obtained the increment data, within the context of a PhD project supervised by ALAJ. BRS and MJL facilitated the isotopic analysis. SG provided shell photographs together with detailed information concerning the stratigraphy and environments of the Belgian and Dutch Pliocene, supplied as comments on the first draft of the paper. BRS and MJL also commented on the first draft.

**Disclaimer.** The contact author has declared that neither they nor their co-authors have any competing interests.

**Acknowledgements.** We thank the following for facilitating study of museum specimens in their care: Annelise Folie, Robert Marquet, and Etienne Steurbaut (Institut royal des Sciences naturelles de Belgique, Brussels, Belgium); Frank Wesselingh (Naturalis Biodiversity Center, Leiden, the Netherlands); and Serge Gofas and Virginie Héros (Muséum National d'Histoire Naturelle, Paris, France). Melita Peharda (Institut za oceanografiju i ribarstvo, Split, Croatia) and Guillermo Roman (Instituto Español de Oceanografía, La Coruña, Spain) generously supplied live-collected individuals. Mark Dean and Matthew Hunt (Geoscience, University of Derby, UK) kindly assisted with specimen preparation, and Michael Maus (Institut für Geowissenschaften, Universität Mainz, Germany) and Hilary Sloane (National Environmental Isotope Facility, British Geological Survey, Keyworth, UK) with isotopic analysis.

**Financial support.** This research was supported by the British Geological Survey (grant no. BUFI S157 for the PhD research of Annemarie M. Valentine), the Alexander von Humboldt-Stiftung (study visit to Mainz by Andrew L. A. Johnson), and the Natural Environment Research Council (Isotope analytical services: grant nos. IP-1108-0509, IP-1155-1109).

**Review statement.** This paper was edited by Bjørg Risebrobakken and reviewed by two anonymous referees.

## References

- Alexandroff, S. J., Butler, P. G., Hollyman, P. R., Schöne, B. R., and Scourse, J. D.: Late Holocene seasonal temperature variability of the western Scottish shelf (St Kilda) recorded in fossil shells of the bivalve *Glycymeris glycymeris*, *Palaeogeogr. Palaeocl.*, 562, 110146, <https://doi.org/10.1016/j.palaeo.2020.110146>, 2021.
- Arthur, M. A., Williams, D. F., and Jones, D. S.: Seasonal temperature-salinity changes and thermocline development in the mid-Atlantic Bight as recorded by the isotopic composition of bivalves, *Geology*, 11, 655–659, [https://doi.org/10.1130/0091-7613\(1983\)11<655:STCATD>2.0.CO;2](https://doi.org/10.1130/0091-7613(1983)11<655:STCATD>2.0.CO;2), 1983.
- Bachem, P. E., Risebrobakken, B., De Schepper, S., and McClymont, E. L.: Highly variable Pliocene sea surface conditions in the Norwegian Sea, *Clim. Past*, 13, 1153–1168, <https://doi.org/10.5194/cp-13-1153-2017>, 2017.
- Bemis, B. E., Spero, H. J., Bijma, J., and Lea, D. W.: Reevaluation of the oxygen isotopic composition of planktonic foraminifera: Experimental results and revised paleotemperature equations, *Paleoceanography*, 13, 150–160, <https://doi.org/10.1029/98PA00070>, 1998.
- Bice, K. L., Arthur, M. A., and Marincovich, L.: Late Paleocene Arctic Ocean shallow-marine temperatures from mollusc stable isotopes, *Paleoceanography*, 11, 241–249, <https://doi.org/10.1029/96PA00813>, 1996.
- Bova, S., Rosenthal, Y., Liu, Z., Godad, S. P., and Yan, M.: Seasonal origin of the thermal maxima at the Holocene and the last interglacial, *Nature*, 589, 548–553, <https://doi.org/10.1038/s41586-020-03155-x>, 2021.
- Briard, J., Pucéat, E., Vennin, E., Daëronc, M., Chavagnac, V., Jaillet, R., Merle, D., and de Rafélis, M.: Seawater paleotemperature and paleosalinity evolution in neritic environments of the Mediterranean margin: Insights from isotope analysis of bivalve shells, *Palaeogeogr. Palaeocl.*, 543, 109582, <https://doi.org/10.1016/j.palaeo.2019.109582>, 2020.
- Buchardt, B. and Simonarson, L. A.: Isotopic palaeotemperatures from the Tjörnes Beds in Iceland: evidence of Pliocene cooling, *Palaeogeogr. Palaeocl.*, 189, 71–95, [https://doi.org/10.1016/S0031-0182\(02\)00594-1](https://doi.org/10.1016/S0031-0182(02)00594-1), 2003.
- Caldarescu, D. E., Sadatzki, H., Andersson, C., Schäfer, P., Fortunato, H., and Meckler, A. N.: Clumped isotope thermometry in bivalve shells: A tool for reconstructing seasonal upwelling, *Geochim. Cosmochim. Ac.*, 294, 174–191, <https://doi.org/10.1016/j.gca.2020.11.019>, 2021.
- Chauvaud, L., Thébaud, J., Clavier, J., Lorrain, A., and Strand, Ø.: What's hiding behind ontogenetic  $\delta^{13}\text{C}$  variations in mollusk shells? New insights from the Great Scallop (*Pecten maximus*), *Estuar. Coast.*, 34, 211–220, <https://doi.org/10.1007/s12237-010-9267-4>, 2011.
- Coplen, T. B., Kendall, C., and Hopple, J.: Comparison of stable isotope reference samples, *Nature*, 302, 236–238, <https://doi.org/10.1038/302236a0>, 1983.
- Crippa, G., Angiolini, L., Bottini, C., Erba, E., Felletti, F., Frigerio, C., Hennissen, J. A. I., Leng, M. J., Petruzzo, M. R., Raffi, I., Raineri, G., and Stephenson, M. H.: Seasonality fluctuations recorded in fossil bivalves during the early Pleistocene: Implications for climate change, *Palaeogeogr. Palaeocl.*, 446, 234–251, <https://doi.org/10.1016/j.palaeo.2016.01.029>, 2016.
- Dearing Crampton-Flood, E., Noorbergen, L. J., Smits, D., Boschman, R. C., Donders, T. H., Munsterman, D. K., ten Veen, J., Peterse, F., Lourens, L., and Sinninghe Damsté, J. S.: A new age model for the Pliocene of the southern North Sea basin: a multi-proxy climate reconstruction, *Clim. Past*, 16, 523–541, <https://doi.org/10.5194/cp-16-523-2020>, 2020.
- Deckers, J., Louwye, S., and Goolaerts, S.: The internal division of the Pliocene Lillo Formation: correlation between Cone Penetration Tests and lithostratigraphic type sections, *Geol. Belg.*, 23, 333–343, <https://doi.org/10.20341/gb.2020.027>, 2020.
- DeLong, K. L., Quinn, T. M., and Taylor, F. W.: Reconstructing twentieth-century sea surface temperature variability in the southwest Pacific: A replication study using multiple coral Sr/Ca records from New Caledonia, *Paleoceanography*, 22, PA4212, <https://doi.org/10.1029/2007PA001444>, 2007.
- DeLong, K. L., Flannery, J. A., Maupin, C. R., Poore, R. Z., and Quinn, T. M.: A coral Sr/Ca calibration and replication study of two massive corals from the Gulf of Mexico, *Palaeogeogr. Palaeocl.*, 307, 117–128, <https://doi.org/10.1016/j.palaeo.2011.05.005>, 2011.
- De Meuter, F. and Laga, P.: Lithostratigraphy and biostratigraphy based on benthonic Foraminifera of the Neogene deposits of northern Belgium, *Bulletin van de Belgische Vereniging voor Geologie*, 85, 133–152, 1976.
- de Nooijer, W., Zhang, Q., Li, Q., Zhang, Q., Li, X., Zhang, Z., Guo, C., Nisancioglu, K. H., Haywood, A. M., Tindall, J. C., Hunter, S. J., Dowsett, H. J., Stepanek, C., Lohmann, G., Otto-Bliesner, B. L., Feng, R., Sohl, L. E., Chandler, M. A., Tan, N., Contoux, C., Ramstein, G., Baatsen, M. L. J., von der Heydt, A. S., Chandan, D., Peltier, W. R., Abe-Ouchi, A., Chan, W.-L., Kamae, Y., and Brierley, C. M.: Evaluation of Arctic warming in mid-Pliocene climate simulations, *Clim. Past*, 16, 2325–2341, <https://doi.org/10.5194/cp-16-2325-2020>, 2020.
- De Schepper, S., Head, M. J., and Louwye, S.: Pliocene dinoflagellate cyst stratigraphy, palaeoecology and sequence stratigraphy of the Tunnel-Canal Dock, Belgium, *Geol. Mag.*, 146, 92–112, <https://doi.org/10.1017/S0016756808005438>, 2009.
- de Winter, N. J., Ullmann, C. V., Sørensen, A. M., Thibault, N., Goderis, S., Van Malderen, S. J. M., Snoeck, C., Goolaerts, S., Vanhaecke, F., and Claeys, P.: Shell chemistry of the boreal Campanian bivalve *Rastellum diluvianum* (Linnaeus, 1767) reveals temperature seasonality, growth rates and life cycle of an extinct Cretaceous oyster, *Biogeosciences*, 17, 2897–2922, <https://doi.org/10.5194/bg-17-2897-2020>, 2020a.
- de Winter, N. J., Vellekoop, J., Clark, A. J., Stassen, P., Speijer, R. P., and Claeys, P.: The giant marine gastropod *Campanile giganteum* (Lamarck, 1804) as a high-resolution archive of seasonality in the Eocene greenhouse world, *Geochem. Geophys. Geosy.*

- 21, e2019GC008794, <https://doi.org/10.1029/2019GC008794>, 2020b.
- de Winter, N. J., Agterhuis, T., and Ziegler, M.: Optimizing sampling strategies in high-resolution paleoclimate records, *Clim. Past*, 17, 1315–1340, <https://doi.org/10.5194/cp-17-1315-2021>, 2021.
- Dowsett, H., Robinson, M., Haywood, A., Salzmann, U., Hill, D., Sohl, L., Chandler, M., Williams, M., Foley, K., and Stoll, D.: The PRISM3D paleoenvironmental reconstruction, *Stratigraphy*, 7, 123–129, 2010.
- Dowsett, H. J., Haywood, A. M., Valdes, P. J., Robinson, M. M., Lunt, D. J., Hill, D., Stoll, D. K., and Foley, K. M.: Sea surface temperatures of the mid-Piacenzian Warm Period: A comparison of PRISM3 and HadCM3, *Palaeogeogr. Palaeoclimatol.*, 309, 83–91, <https://doi.org/10.1016/j.palaeo.2011.03.016>, 2011.
- Dowsett, H. J., Robinson, M. M., Stoll, D. K., Foley, K. M., Johnson, A. L. A., Williams, M., and Riesselman, C. R.: The PRISM (Pliocene palaeoclimate) reconstruction: time for a paradigm shift, *Philos. T. Roy. Soc. A*, 371, 20120524, <https://doi.org/10.1098/rsta.2012.0524>, 2013.
- Dowsett, H. J., Robinson, M. M., Foley, K. M., Herbert, T. D., Otto-Bliesner, B. L., and Spivey, W.: The mid-Piacenzian of the North Atlantic Ocean, *Stratigraphy*, 16, 119–144, <https://doi.org/10.29041/strat.16.3.119-144>, 2019.
- Dowsett, H. J., Robinson, M. M., Foley, K. M., and Herbert, T. D.: The Yorktown Formation: Improved stratigraphy, chronology, and paleoclimate interpretations from the U.S. Mid-Atlantic Coastal Plain, *Geosciences*, 11, 486, <https://doi.org/10.3390/geosciences11120486>, 2021.
- Featherstone, A. M., Butler, P. G., Schöne, B. R., Peharda, M., and Thébaud, J.: A 45-year sub-annual reconstruction of seawater temperature in the Bay of Brest, France, using the shell oxygen isotope composition of the bivalve *Glycymeris glycymeris*, *Holocene*, 30, 3–12, <https://doi.org/10.1177/0959683619865592>, 2020.
- Fenger, T., Surge, D., Schöne, B. R., and Milner, N.: Sclerochronology and geochemical variation in limpet shells (*Patella vulgata*): A new archive to reconstruct coastal sea surface temperature, *Geochem. Geophys. Geosy.*, 8, Q07001, <https://doi.org/10.1029/2006GC001488>, 2007.
- Füllenbach, C. S., Schöne, B. R., and Mertz-Kraus, R.: Strontium/lithium ratio in shells of *Cerastoderma edule* (Bivalvia) – A new potential temperature proxy for brackish environments, *Chem. Geol.*, 417, 341–355, <https://doi.org/10.1016/j.chemgeo.2015.10.030>, 2015.
- Funnell, B. M.: Plio-Pleistocene palaeogeography of the southern North Sea Basin (3.75–0.60 Ma), *Quaternary Sci. Rev.*, 15, 391–405, [https://doi.org/10.1016/0277-3791\(96\)00022-4](https://doi.org/10.1016/0277-3791(96)00022-4), 1996.
- Gaemers, P. A. M.: Enkele paleo-ecologische opmerkingen over de Pliocene afzettingen in de tunnelput nabij Kallo, België, provincie Oost-Vlaanderen. Deel 2, Mededelingen van de Werkgroep voor Tertiäre en Kwartaire Geologie, 12, 43–49, 1975.
- Gaemers, P. A. M. and Schwarzhans, W.: Fisch-Otolithen aus dem Pliozän von Antwerpen (Belgien) und Ouwerkerk (Niederlande) und aus dem Plio-Pleistozän der Westerschelde (Niederlande), *Leidse Geologische Mededelingen*, 49, 207–257, 1973.
- Garcia-March, J. R., Surge, D., Lees, J. M., and Kersting, D. K.: Ecological information and water mass properties in the Mediterranean recorded by stable isotope ratios in *Pinna nobilis* shells, *J. Geophys. Res.*, 116, G02009, <https://doi.org/10.1029/2010JG001461>, 2011.
- Gibbard, P. L. and Lewin, J.: Filling the North Sea Basin: Cenozoic sediment sources and river styles (André Dumont medallist lecture 2014), *Geol. Belg.*, 19, 201–217, <https://doi.org/10.20341/gb.2015.017>, 2016.
- Gillikin, D. P., Lorrain, A., Navez, J., Taylor, J. W., Keppens, E., Baeyens, W., and Dehairs, F.: Strong biological controls on Sr/Ca ratios in aragonitic marine bivalve shells, *Geochem. Geophys. Geosy.*, 6, Q05009, <https://doi.org/10.1029/2004GC000874>, 2005.
- Goodwin, D. H., Schöne, B. R., and Dettman, D. L.: Resolution and fidelity of oxygen isotopes as paleotemperature proxies in bivalve mollusk shells: Models and observations, *Palaios*, 18, 110–125, [https://doi.org/10.1669/0883-1351\(2003\)18<110:RAFOOI>2.0.CO;2](https://doi.org/10.1669/0883-1351(2003)18<110:RAFOOI>2.0.CO;2), 2003.
- Grossman, E. L. and Ku, T.: Oxygen and carbon isotope fractionation in biogenic aragonite: Temperature effects, *Chemical Geology: Isotope Geoscience section*, 59, 59–74, [https://doi.org/10.1016/0009-2541\(86\)90044-6](https://doi.org/10.1016/0009-2541(86)90044-6), 1986.
- Hacquart, N.: Palynologisch onderzoek van de cenozoische mariene zanden (Scaldisien en Merxemian) van het Hansadok te Antwerpen, *Natuurwetenschappelijk Tijdschrift*, 42, 65–112, 1960.
- Harwood, A. J. P., Dennis, P. F., Marca, A. D., Pilling, G. M., and Millner, R. S.: The oxygen isotope composition of water masses within the North Sea, *Estuar. Coast. Shelf S.*, 78, 353–359, <https://doi.org/10.1016/j.ecss.2007.12.010>, 2008.
- Haywood, A. M., Sellwood, B. W., and Valdes, P. J.: Regional warming: Pliocene (3Ma) paleoclimate of Europe and the Mediterranean, *Geology*, 28, 1063–1066, 2000.
- Hennissen, J. A. I., Head, M. J., De Schepper, S., and Groeneveld, J.: Increased seasonality during the intensification of Northern Hemisphere glaciation at the Pliocene-Pleistocene boundary ~2.6 Ma, *Quaternary Sci. Rev.*, 129, 321–332, <https://doi.org/10.1016/j.quascirev.2015.10.010>, 2015.
- Hennissen, J. A. I., Head, M. J., De Schepper, S., and Groeneveld, J.: Dinoflagellate cyst paleoecology during the Pliocene–Pleistocene climatic transition in the North Atlantic, *Palaeogeogr. Palaeoclimatol.*, 470, 81–108, <https://doi.org/10.1016/j.palaeo.2016.12.023>, 2017.
- Hickson, J. A., Johnson, A. L. A., Heaton, T. H. E., and Balson, P. S.: The shell of the Queen Scallop *Aequipecten opercularis* (L.) as a promising tool for palaeoenvironmental reconstruction: evidence and reasons for equilibrium stable-isotope incorporation, *Palaeogeogr. Palaeoclimatol.*, 154, 325–337, [https://doi.org/10.1016/S0031-0182\(99\)00120-0](https://doi.org/10.1016/S0031-0182(99)00120-0), 1999.
- Hickson, J. A., Johnson, A. L. A., Heaton, T. H. E., and Balson, P. S.: Late Holocene environment of the southern North Sea from the stable isotopic composition of Queen Scallop shells, *Palaeontol. Electron.*, 3, 11 pp., [https://palaeo-electronica.org/2000\\_2/scallop/issue2\\_00.htm](https://palaeo-electronica.org/2000_2/scallop/issue2_00.htm) (last access: 17 May 2022), 2000.
- Höche, N., Peharda, M., Walliser, E. O., and Schöne, B. R.: Morphological variations of crossed-lamellar ultrastructures of *Glycymeris bimaculata* (Bivalvia) serve as a marine temperature proxy, *Estuar. Coast. Shelf S.*, 237, 106658, <https://doi.org/10.1016/j.ecss.2020.106658>, 2020.
- Höche, N., Walliser, E. O., de Winter, N. J., Witbaard, R., and Schöne, B. R.: Temperature-induced mi-

- crostructural changes in shells of laboratory-grown *Arctica islandica* (Bivalvia), *PloS ONE*, 16, e0247968, <https://doi.org/10.1371/journal.pone.0247968>, 2021.
- Howarth, M. J., Dyer, K. R., Joint, I. R., Hydes, D. J., Purdie, D. A., Edmunds, H., Jones, J. E., Lowry, R. K., Mofatt, T. J., Pomroy, A. J., and Proctor, R.: Seasonal cycles and their spatial variability, *Philos. T. Roy. Soc. A*, 343, 383–403, <https://doi.org/10.1098/rsta.1993.0054>, 1993.
- Huyghe, D., Emmanuel, L., de Rafelis, M., Renard, M., Ropert, M., Labourdette, N., and Lartaud, F.: Oxygen isotope disequilibrium in the juvenile portion of oyster shells biases seawater temperature reconstructions, *Estuar. Coast. Shelf Sci.*, 240, 106777, <https://doi.org/10.1016/j.ecss.2020.106777>, 2020.
- Huyghe, D., Daëron, M., de Rafelis, M., Blamart, D., Sébilo, M., Paulet, Y.-M., and Lartaud, F.: Clumped isotopes in modern marine bivalves, *Geochim. Cosmochim. Ac.*, 316, 41–58, <https://doi.org/10.1016/j.gca.2021.09.019>, 2022.
- Ivany, L. C. and Judd, E. J.: Deciphering temperature seasonality in Earth's ancient oceans, *Annu. Rev. Earth Planet. Sci.*, 50, 123–152, <https://doi.org/10.1146/annurev-earth-032320-095156>, 2022.
- Ivany, L. C., Wilkinson, B. H., and Jones, D. S.: Using stable isotope data to resolve rate and duration of growth throughout ontogeny: An example from the surf clam, *Spisula solidissima*, *Palaios*, 18, 126–137, [https://doi.org/10.1669/0883-1351\(2003\)18<126:USIDTR>2.0.CO;2](https://doi.org/10.1669/0883-1351(2003)18<126:USIDTR>2.0.CO;2), 2003.
- Ivany, L. C., Wilkinson, B. H., Lohmann, K. C., Johnson, E. R., McElroy, B. J., and Cohen, G. J.: Intra-annual isotopic variation in *Venericardia* bivalves: Implications for early Eocene temperature, seasonality, and salinity on the US Gulf Coast, *J. Sediment. Res.*, 74, 7–19, <https://doi.org/10.1306/052803740007>, 2004.
- Johnson, A. L. A., Hickson, J. A., Bird, A., Schöne, B. R., Balson, P. S., Heaton, T. H. E., and Williams, M.: Comparative sclerochronology of modern and mid-Pliocene (c. 3.5 Ma) *Aequipecten opercularis* (Mollusca, Bivalvia): an insight into past and future climate change in the northeast Atlantic region, *Palaeogeogr. Palaeoclimatol.*, 284, 164–179, <https://doi.org/10.1016/j.palaeo.2009.0.022>, 2009.
- Johnson, A. L. A., Valentine, A., Leng, M. J., Sloane, H. J., Schöne, B. R., and Balson, P. S.: Isotopic temperatures from the Early and Mid-Pliocene of the US Middle Atlantic Coastal Plain, and their implications for the cause of regional marine climate change, *Palaios*, 32, 250–269, <https://doi.org/10.2110/palo.2016.080>, 2017.
- Johnson, A. L. A., Valentine, A. M., Leng, M. J., Schöne, B. R., and Sloane, H. J.: Life history, environment and extinction of the scallop *Carolinapecten eboeus* (Conrad) in the Plio-Pleistocene of the US eastern seaboard, *Palaios*, 34, 49–70, <https://doi.org/10.2110/palo.2018.056>, 2019.
- Johnson, A. L. A., Harper, E. M., Clarke, A., Featherstone, A. C., Heywood, D. J., Richardson, K. E., Spink, J. O., and Thornton, L. A. H.: Growth rate, extinction and survival amongst late Cenozoic bivalves of the North Atlantic, *Hist. Biol.*, 33, 802–813, <https://doi.org/10.1080/08912963.2019.1663839>, 2021a.
- Johnson, A. L. A., Valentine, A. M., Schöne, B. R., Leng, M. J., Sloane, H. J., and Janeković, I.: Growth-increment characteristics and isotopic ( $\delta^{18}\text{O}$ ) temperature record of sub-thermocline *Aequipecten opercularis* (Mollusca:Bivalvia): evidence from modern Adriatic forms and an application to early Pliocene examples from eastern England, *Palaeogeogr. Palaeoclimatol.*, 561, 110046, <https://doi.org/10.1016/j.palaeo.2020.110046>, 2021b.
- Johnson, A. L. A., Valentine, A. M., Schöne, B. R., Leng, M. J., Sloane, H. J., and Goolaerts, S.: Raw data for “Sclerochronological evidence of pronounced seasonality from the late Pliocene of the southern North Sea Basin, and its implications”, Version 1, Zenodo [data set], <https://doi.org/10.5281/zenodo.5585630>, 2021c.
- Kim, S.-T. and O’Neil, J. R.: Equilibrium and nonequilibrium oxygen isotope effects in synthetic carbonates, *Geochim. Cosmochim. Ac.*, 61, 3461–3475, [https://doi.org/10.1016/S0016-7037\(97\)00169-5](https://doi.org/10.1016/S0016-7037(97)00169-5), 1997.
- Kim, S.-T., O’Neil, J. R., Hillaire-Marcel, C., and Mucci, A.: Oxygen isotope fractionation between synthetic aragonite and water: Influence of temperature and  $\text{Mg}^{2+}$  concentration, *Geochim. Cosmochim. Ac.*, 71, 4704–4715, <https://doi.org/10.1016/j.gca.2007.04.019>, 2007.
- Knowles, T., Taylor, P. D., Williams, M., Haywood, A. M., and Okamura, B.: Pliocene seasonality across the North Atlantic inferred from cheilostome bryozoans, *Palaeogeogr. Palaeoclimatol.*, 77, 226–235, <https://doi.org/10.1016/j.palaeo.2009.04.006>, 2009.
- Krantz, D. E., Williams, D. F., and Jones, D. S.: Ecological and paleoenvironmental information using stable isotope profiles from living and fossil molluscs, *Palaeogeogr. Palaeoclimatol.*, 58, 249–266, [https://doi.org/10.1016/0031-0182\(87\)90064-2](https://doi.org/10.1016/0031-0182(87)90064-2), 1987.
- Laga, P.: Stratigrafie van de mariene Plio-Pleistocene afzettingen uit de omgeving van Antwerpen met een bijzondere studie van de foraminiferen, PhD thesis, Katholieke Universiteit Leuven, Belgium, 252 pp., 1972.
- Lane, A. and Prandle, D.: Inter-annual variability in the temperature of the North Sea, *Cont. Shelf Res.*, 16, 1489–1507, [https://doi.org/10.1016/0278-4343\(96\)00001-5](https://doi.org/10.1016/0278-4343(96)00001-5), 1996.
- Lisiecki, L. E. and Raymo, M. E.: A Pliocene–Pleistocene stack of 57 globally distributed benthic  $\delta^{18}\text{O}$  records, *Paleoceanography*, 20, 522–533, <https://doi.org/10.1029/2004PA001071>, 2005.
- Lloyd, R. M.: Variations in the oxygen and carbon isotope ratios of Florida Bay mollusks and their environmental significance, *J. Geol.*, 72, 84–111, 1964.
- Lorrain, A., Paulet, Y.-M., Chauvaud, L., Dunbar, R., Mucciaroni, D., and Fontugne, M.:  $\delta^{13}\text{C}$  variation in scallop shells: Increasing metabolic carbon contribution with body size?, *Geochim. Cosmochim. Ac.*, 68, 3509–3519, <https://doi.org/10.1016/j.gca.2004.01.025>, 2004.
- Louwey, S. and De Schepper, S.: The Miocene-Pliocene hiatus in the southern North Sea Basin (northern Belgium) revealed by dinoflagellate cysts, *Geol. Mag.*, 147, 760–776, <https://doi.org/10.1017/S0016756810000191>, 2010.
- Louwey, S., Head, M. J., and De Schepper, S.: Dinoflagellate cyst stratigraphy and palaeoecology of the Pliocene in northern Belgium, southern North Sea Basin, *Geol. Mag.*, 141, 353–378, <https://doi.org/10.1017/S0016756804009136>, 2004.
- Louwey, S., Deckers, J., and Vandenberghe, N.: The Pliocene Lillo, Poederlee, Merksplas, Mol and Kieseloolite Formations in northern Belgium: a synthesis, *Geol. Belg.*, 23, 297–313, <https://doi.org/10.20341/gb.2020.016>, 2020.
- Lunt, D. J., Haywood, A. M., Schmidt, G. A., Salzmann, U., Valdes, P. J., and Dowsett, H. J.: Earth system sensitivity inferred from Pliocene modelling and data, *Nat. Geosci.*, 3, 60–64, <https://doi.org/10.1038/ngeo706>, 2010.

- Marchais, V., Richard, J., Jolivet, A., Flye-Sainte-Marie, J., Thébault, J., Jean, F., Richard, P., Paulet, Y.-M., Clavier, J., and Chauvaud, L.: Coupling experimental and field-based approaches to decipher carbon sources in the shell of the great scallop, *Pecten maximus* (L.), *Geochim. Cosmochim. Ac.*, 168, 58–69, <https://doi.org/10.1016/j.gca.2015.07.010>, 2015.
- Markulin, K., Peharda, M., Mertz-Kraus, R., Schöne, B. R., Uvanović, H., Kovač, Z., and Janeković, I.: Trace and minor element records in aragonitic bivalve shells as environmental proxies, *Chem. Geol.*, 507, 120–133, <https://doi.org/10.1016/j.chemgeo.2019.01.008>, 2019.
- Marquet, R.: The Neogene Amphineura and Bivalvia (Protobranchia and Pteriomorpha) from Kallo and Doel (Oost-Vlaanderen, Belgium), *Palaeontos*, 2, 1–99, 2002.
- Marquet, R.: Ecology and evolution of Pliocene bivalves from the Antwerp Basin, *Bulletin de l'Institut Royal des Sciences Naturelles de Belgique*, 74, 205–212, 2004.
- Marquet, R.: The Neogene Bivalvia (Heterodonta and Anomalodesmata) and Scaphopoda from Kallo and Doel (Oost-Vlaanderen, Belgium), *Palaeontos*, 6, 1–142, 2005.
- Marquet, R. and Herman, J.: The stratigraphy of the Pliocene in Belgium, *Palaeofocus*, 2, 1–39, 2009.
- Mettam, C., Johnson, A. L. A., Nunn, E. V., and Schöne, B. R.: Stable isotope ( $\delta^{18}\text{O}$  and  $\delta^{13}\text{C}$ ) sclerochronology of Callovian (Middle Jurassic) bivalves (*Gryphaea* (*Bilobissa*) *dilobotes*) and belemnites (*Cylindroteuthis puzosiana*) from the Peterborough Member of the Oxford Clay Formation (Cambridgeshire, England): evidence of palaeoclimate, water depth and belemnite behaviour, *Palaeogeogr. Palaeoclimatol.*, 399, 187–201, <https://doi.org/10.1016/j.palaeo.2014.01.010>, 2014.
- Mette, M. J., Whitney, N. M., Ballew, J., and Wanamaker, A. D.: Unexpected isotopic variability in biogenic aragonite: A user issue or proxy problem?, *Chem. Geol.*, 483, 286–294, <https://doi.org/10.1016/j.chemgeo.2018.02.027>, 2018.
- Moon, L. R., Judd, E. J., Thomas, J., and Ivany, L. C.: Out of the oven and into the fire: Unexpected preservation of the seasonal  $\delta^{18}\text{O}$  cycle following heating experiments on shell carbonate, *Palaeogeogr. Palaeoclimatol.*, 562, 110115, <https://doi.org/10.1016/j.palaeo.2020.110115>, 2021.
- Munsterman, D. K., ten Veen, J. H., Menkovic, A., Deckers, J., Witmans, N., Verhaegen, J., Kersthoud-Boegehold, S. J., van de Ven, T., and Busschers, F.: An updated and revised stratigraphic framework for the Miocene and earliest Pliocene strata of the Roer Valley Graben and adjacent blocks, *Neth. J. Geosci.*, 98, E8, <https://doi.org/10.1017/njg.2019.10>, 2020.
- Murray, J. W.: Palaeogene and Neogene, in: *Atlas of Palaeogeography and Lithofacies*, edited by: Cope, J. C. W., Ingham, J. K., and Rawson, P. F., The Geological Society, London, UK, Memoir 13, 141–147, 1992.
- Nooitgedacht, C. W., van der Lubbe, H. J. L., Ziegler, M., and Staudigel, P. T.: Internal water facilitates thermal resetting of clumped isotopes in biogenic aragonite, *Geochem. Geophys. Geosyst.*, 22, e2021GC009730, <https://doi.org/10.1029/2021GC009730>, 2021.
- Norton, P. E. P.: Paleoecology of the Mollusca of the Tjörnes sequence, Iceland, *Boreas*, 4, 97–110, 1975.
- O'Neil, J. R., Clayton, R. N., and Mayeda, T. K.: Oxygen isotope fractionation in divalent metal carbonates, *J. Chem. Phys.*, 51, 5547–5558, 1969.
- Overeem, I., Weltje, G. J., Bishop-Kay, C., and Kroonenberg, S. B.: The Late Cenozoic Eridanos delta system in the Southern North Sea Basin: a climate signal in sediment supply?, *Basin Res.*, 13, 293–312, <https://doi.org/10.1046/j.1365-2117.2001.00151.x>, 2001.
- Owen, R., Kennedy, H., and Richardson, C.: Isotopic partitioning between scallop shell calcite and seawater: Effect of shell growth rate, *Geochim. Cosmochim. Ac.*, 66, 1727–1737, [https://doi.org/10.1016/S0016-7037\(01\)00882-1](https://doi.org/10.1016/S0016-7037(01)00882-1), 2002a.
- Owen, R., Kennedy, H., and Richardson, C.: Experimental investigation into partitioning of stable isotopes between scallop (*Pecten maximus*) shell calcite and sea water, *Palaeogeogr. Palaeoclimatol.*, 185, 163–174, [https://doi.org/10.1016/S0031-0182\(02\)00297-3](https://doi.org/10.1016/S0031-0182(02)00297-3), 2002b.
- Panitz, S., Salzmann, U., Risebrobakken, B., De Schepper, S., Pound, M. J., Haywood, A. M., Dolan, A. M., and Lunt, D. J.: Orbital, tectonic and oceanographic controls on Pliocene climate and atmospheric circulation in Arctic Norway, *Global Planet. Change*, 161, 183–193, <https://doi.org/10.1016/j.gloplacha.2017.12.022>, 2018.
- Peharda, M., Crnčević, M., Bušelić, I., Richardson, C. A., and Ezgeta-Balić, D.: Growth and longevity of *Glycymeris nummaria* (Linnaeus, 1758) from the eastern Adriatic, Croatia, *J. Shellfish Res.*, 31, 947–950, <https://doi.org/10.2983/035.031.0406>, 2012.
- Peharda, M., Thébault, J., Markulin, K., Schöne, B. R., Janeković, I., and Chauvaud, L.: Contrasting shell growth strategies in two Mediterranean bivalves revealed by oxygen-isotope ratio geochemistry: The case of *Pecten jacobaeus* and *Glycymeris pilosa*, *Chem. Geol.*, 526, 23–35, <https://doi.org/10.1016/j.chemgeo.2017.09.029>, 2019a.
- Peharda, M., Walliser, E. O., Markulin, K., Purroy, A., Uvanović, H., Janeković, I., Župan, I., Vilibić, I., and Schöne, B. R.: *Glycymeris pilosa* (Bivalvia) – A high-potential geochemical archive of the environmental variability in the Adriatic Sea, *Mar. Environ. Res.*, 150, 104759, <https://doi.org/10.1016/j.marenvres.2019.104759>, 2019b.
- Raffi, S., Stanley, S. M., and Marasti, R.: Biogeographic patterns and Plio-Pleistocene extinction of Bivalvia in the Mediterranean and southern North Sea, *Paleobiology*, 11, 368–388, <https://doi.org/10.1017/S0094837300011684>, 1985.
- Reynolds, D. J., Hall, I. R., Slater, S. M., Scourse, J. D., Halloran, P. R., and Sayer, M. D. J.: Reconstructing past seasonal to multicentennial-scale variability in the NE Atlantic Ocean using the long-lived marine bivalve mollusk *Glycymeris glycymeris*, *Paleoceanography*, 32, 1153–1173, <https://doi.org/10.1002/2017PA003154>, 2017.
- Robinson, M. M.: New quantitative evidence of extreme warmth in the Pliocene Arctic, *Stratigraphy*, 6, 265–275, 2009.
- Robinson, M. M., Dowsett, H. J., Foley, K. M., and Riesselman, C. R.: PRISM marine sites: The history of PRISM sea surface temperature estimation, U.S. Geological Survey Open-File Report, 2018–1148, 49 pp., <https://doi.org/10.3133/ofr20181148>, 2018.
- Royer, C., Thébault, J., Chauvaud, L., and Olivier, F.: Structural analysis and paleoenvironmental potential of dog cockle shells (*Glycymeris glycymeris*) in Brittany, northwest France, *Palaeogeogr. Palaeoclimatol.*, 373, 123–132, <https://doi.org/10.1016/j.palaeo.2012.01.033>, 2013.
- Schöne, B. R.: The curse of physiology—challenges and opportunities in the interpretation of geochemical data from mollusk shells,

- Geo-Mar. Lett., 28, 269–285, <https://doi.org/10.1007/s00367-008-0114-6>, 2008.
- Schöne, B. R.: *Arctica islandica* (Bivalvia): A unique paleoenvironmental archive of the northern North Atlantic Ocean, *Global Planet. Change*, 111, 199–225, <https://doi.org/10.1016/j.gloplacha.2013.09.013>, 2013.
- Schöne, B. R. and Fiebig, J.: Seasonality in the North Sea during the Allerød and Late Medieval Climate Optimum using bivalve sclerochronology, *Int. J. Earth Sci.*, 98, 83–98, <https://doi.org/10.1007/s00531-008-0363-7>, 2009.
- Schöne, B. R., Fiebig, J., Pfeiffer, M., Gleß, R., Hickson, J., Johnson, A. L. A., Dreyer, W., and Oschmann, W.: Climate records from a bivalved *Methuselah* (*Arctica islandica*, Mollusca; Iceland), *Palaeogeogr. Palaeoclimatol.*, 228, 130–148, <https://doi.org/10.1016/j.palaeo.2005.03.049>, 2005.
- Shackleton, N. J.: Attainment of isotopic equilibrium between ocean water and the benthonic foraminifera genus *Uvigerina*: Isotopic changes in the ocean during the last glacial, *Colloques Internationaux du Centre National de la Recherche Scientifique*, 219, 203–209, 1974.
- Slupik, A. A., Wesselingh, F. P., Janse, A. C., and Reumer, J. W. F.: The stratigraphy of the Neogene-Quaternary succession in the southwest Netherlands from the Schelphoek borehole (42G4-11/42G0022) – a sequence stratigraphic approach, *Neth. J. Geosci.*, 86, 317–332, <https://doi.org/10.1017/S0016774600023556>, 2007.
- Surge, D. and Barrett, J. H.: Marine climatic seasonality during medieval times (10th to 12th centuries) based on isotopic records in Viking Age shells from Orkney, Scotland, *Palaeogeogr. Palaeoclimatol.*, 350, 236–246, <https://doi.org/10.1016/j.palaeo.2012.07.003>, 2012.
- Tebble, N.: *British Bivalve Seashells*, 2nd edn., Her Majesty's Stationary Office, Edinburgh, UK, 212 pp., ISBN 0 11 491401 X, 1976.
- Trofimova, T., Milano, S., Andersson, C., Bonitz, F. G. W., and Schöne, B. R.: Oxygen isotope composition of *Arctica islandica* aragonite in the context of shell architectural organization: Implications for paleoclimate reconstructions, *Geochem. Geophys. Geosy.*, 19, 453–470, <https://doi.org/10.1002/2017GC007239>, 2018.
- Ullmann, C. V., Wiechert, U., and Korte, C.: Oxygen isotope fluctuations in a modern North Sea oyster (*Crassostrea gigas*) compared with annual variations in seawater temperature: Implications for palaeoclimate studies, *Chem. Geol.*, 270, 170–176, <https://doi.org/10.1016/j.chemgeo.2010.07.019>, 2010.
- Valentine, A., Johnson, A. L. A., Leng, M. J., Sloane, H. J., and Balson, P. S.: Isotopic evidence of cool winter conditions in the mid-Piacenzian (Pliocene) of the southern North Sea Basin, *Palaeogeogr. Palaeoclimatol.*, 309, 9–16, <https://doi.org/10.1016/j.palaeo.2011.05.015>, 2011.
- Vandenbergh, N., Herman, J., Laga, P., Louwey, S., De Schepper, S., Vandenbergh, J., Bohncke, S., and Konert, W.: The stratigraphic position of a Pliocene tidal clay deposit at Grobbendonk (Antwerp Province, Belgium), *Geol. Belg.*, 3, 405–17, <https://doi.org/10.20341/gb.2014.040>, 2000.
- Van Vliet-Lanoë, B., Vandenbergh, N., Laurent, M., Laignel, B., Lauriat-Rage, A., Louwey, S., Mansy, J.-L., Mercier, D., Halégouët, B., Laga, P., Laquement, F., Melliez, F., Michel, Y., Mougedet, G., and Villier, J.-P.: Palaeogeographic evolution of northwestern Europe during the Upper Cenozoic, in: *Messinia event: palaeobiological and palaeoecological approaches*: edited by: Néraudeau, D. and Goubert, É., *Geodiversitas*, 24, 511–541, 2002.
- Vignols, R. M., Valentine, A. M., Finlayson, A. G., Harper, E. M., Schöne, B. R., Leng, M. J., Sloane, H. J., and Johnson, A. L. A.: Marine climate and hydrography of the Coralline Crag (early Pliocene, UK): isotopic evidence from 16 benthic invertebrate taxa, *Chem. Geol.*, 536, 62–83, <https://doi.org/10.1016/j.chemgeo.2018.05.034>, 2019.
- Wesselingh, F. P., Busschers, F. S., and Goolaerts, S.: Observations on the Pliocene sediments exposed at Antwerp International Airport (northern Belgium) constrain the stratigraphic position of the Broechem fauna, *Geol. Belg.*, 23, 315–321, <https://doi.org/10.20341/gb.2020.026>, 2020.
- Westaway, R., Maddy, D., and Bridgland, D.: Flow in the lower continental crust as a mechanism for the Quaternary uplift of southeast England: constraints from the Thames terrace record, *Quaternary Sci. Rev.*, 21, 559–603, [https://doi.org/10.1016/S0277-3791\(01\)00040-3](https://doi.org/10.1016/S0277-3791(01)00040-3), 2002.
- Williams, M., Haywood, A. M., Harper, E. M., Johnson, A. L. A., Knowles, T., Leng, M. J., Lunt, D. J., Okamura, B., Taylor, P. D., and Zaliziewicz, J.: Pliocene climate and seasonality in North Atlantic shelf seas, *Philos. T. Roy. Soc. A*, 367, 85–108, <https://doi.org/10.1098/rsta.2008.0224>, 2009.
- Williams, M., Nelson, A. E., Smellie, J. L., Leng, M. J., Johnson, A. L. A., Jarram, D. R., Haywood, A. M., Peck, V. L., Zalasiewicz, J., Bennett, C., and Schöne, B. R.: Sea ice extent and seasonality for the Early Pliocene northern Weddell Sea determined from fossil *Austrochlamys* bivalves, *Palaeogeogr. Palaeoclimatol.*, 292, 306–318, <https://doi.org/10.1016/j.palaeo.2010.04.003>, 2010.
- Winther, N. G. and Johannessen, J. A.: North Sea circulation: Atlantic inflow and its destination, *J. Geophys. Res.*, 111, C12018, <https://doi.org/10.1029/2005JC003310>, 2006.
- Witbaard, R. and Bergman, M. J. N.: The distribution and population structure of the bivalve *Arctica islandica* L. in the North Sea: what possible factors are involved?, *J. Sea Res.*, 50, 11–25, [https://doi.org/10.1016/S1385-1101\(03\)00039-X](https://doi.org/10.1016/S1385-1101(03)00039-X), 2003.
- Wood, A. M., Wilkinson, I. P., Maybury, C. A., and Whatley, R. C.: Neogene, in: *Ostracods in British Stratigraphy*, edited by: Whitaker, J. E. and Hart, M. B., *Spec. Publ., The Micropalaeontological Society, The Geological Society, London, UK*, 411–446, ISSN 1747-602X, 2009.
- Wood, A. M., Whatley, R. C., Cronin, T., and Holtz, T.: Pliocene palaeotemperature reconstruction for the southern North Sea based on Ostracoda, *Quaternary Sci. Rev.*, 12, 747–767, [https://doi.org/10.1016/0277-3791\(93\)90015-E](https://doi.org/10.1016/0277-3791(93)90015-E), 1993.
- Zhang, Z., Li, X., Guo, C., Otterå, O. H., Nisancioglu, K. H., Tan, N., Contoux, C., Ramstein, G., Feng, R., Otto-Bliesner, B. L., Brady, E., Chandan, D., Peltier, W. R., Baatsen, M. L. J., von der Heydt, A. S., Weiffenbach, J. E., Stepanek, C., Lohmann, G., Zhang, Q., Li, Q., Chandler, M. A., Sohl, L. E., Haywood, A. M., Hunter, S. J., Tindall, J. C., Williams, C., Lunt, D. J., Chan, W.-L., and Abe-Ouchi, A.: Mid-Pliocene Atlantic Meridional Overturning Circulation simulated in PlioMIP2, *Clim. Past*, 17, 529–543, <https://doi.org/10.5194/cp-17-529-2021>, 2021.